STANFORD RESEARCH INSTITUTE
Menlo Park, California 94025 • U.S.A.

Final Report *March 1976*

FEASIBILITY OF AN INCOHERENT-SCATTER RADAR ABOARD THE SPACE SHUTTLE

By: M. BARON R. TSUNODA J. PETRICEKS H. KUNNES

Prepared for:

UNIVERSITY OF CALIFORNIA
BERKELEY, CALIFORNIA 94720
Attention: DR. FORREST S. MOZER

CONTRACT P.O. G704210

SRI Project 4278

Approved by:

DAVID A. JOHNSON, *Director*
Radio Physics Laboratory

RAY L. LEADABRAND, *Executive Director*
Electronics and Radio Sciences Division

NOV 1976
RECEIVED

N77-10400

(NASA-CR-144336) FEASIBILITY OF AN INCOHERENT-SCATTER RADAR ABOARD THE SPACE SHUTTLE Final Report (Stanford Research Inst.) 100 p HC A05/MF A01 CSCL 17I
Unclas
G3/32 09633

Copy No. 12

ABSTRACT

The results of a preliminary study to investigate the feasibility of conducting an incoherent-scatter radar experiment on board the Space Shuttle are presented in this report. The results indicate that such an experiment is technically feasible. The more difficult questions to answer are whether the system can be made flexible enough to justify the problems and costs involved. In this report, we evaluate the design parameters and the tradeoffs that are available in the consideration of these questions.

Some of the more serious limitations pertain to: (1) the presence of ground clutter and F-region auroral clutter; (2) available average power; (3) weight and volume associated with required antenna size, transmitter, and energy storage devices; and (4) antenna breakdown associated with high-power transmitter problems.

CONTENTS

ABSTRACT iii

LIST OF ILLUSTRATIONS vii

LIST OF TABLES ix

1. INTRODUCTION 1

2. SIGNAL-TO-NOISE-RATIO ESTIMATION 3

2.1 Signal Power 3

2.2 Noise-Power Calculation 6

2.2.1 System Noise Temperature 6

2.2.2 Bandwidth Requirements 7

2.2.3 Total Noise Power 10

2.3 Signal-to-Noise Ratio 10

2.3.1 λ, τ Dependence 12

2.3.2 Power-Aperture Requirement 14

3. WAVEFORM DESIGN 17

3.1 General 17

3.2 Two Possible Waveforms 21

4. TRADEOFFS AND CONSTRAINTS 27

4.1 Utilization of Available Power 28

4.2 Clutter 30

4.2.1 Mainlobe Ground Clutter 30

4.2.1.1 Case 1: Grazing Incidence 31

4.2.1.2 Case 2: Steep Incidence 33

4.2.2 Sidelobe Ground Clutter 34

4.2.3 Auroral Clutter 35

4.2.4 Clutter Mitigation 38

PRECEDING PAGE BLANK NOT FILMED

4. Continued

4.3 Averaging Time vs Spatial Resolution 40

4.4 Transmitter 43

4.5 Energy-Storage Considerations 46

4.6 Antenna 48

4.6.1 Antenna Size and Weight 48

4.6.2 Antenna Deployment and Steering Considerations . 49

4.6.3 Atmospheric Drag on Large-Aperture Antennas . . . 51

4.7 Antenna Breakdown Considerations 54

4.7.1 Gas Discharge Breakdown 56

4.7.2 Field-Emission Effects 59

4.7.3 Multipactor Discharges 61

4.8 Phased-Array Antenna 61

5. SEMICOHERENT BACKSCATTER STUDIES 67

5.1 E-Region Irregularities 67

5.1.1 Equatorial Backscatter Studies 68

5.1.2 Auroral Backscatter Studies 69

5.1.3 Polar Cap Backscatter Studies 71

5.2 F-Region Irregularities 72

6. DISCUSSION 75

7. RECOMMENDATIONS FOR FUTURE STUDY 79

REFERENCES 81

ILLUSTRATIONS

2.1 Cosmic Noise and Receiver Temperatures vs Frequency 8

2.2 Total Noise Power vs Frequency 11

2.3 SNR Dependence on λ, τ 13

2.4 Power-Aperture-Product Requirement 15

3.1 The T_r Variation of the Power Spectra and Autocorrelation Functions (ACFs) 19

3.2 The T_i Variation of the Power Spectra and ACFs 20

3.3 Single-Pulse Range-Time Representation 22

3.4 Pulse-Burst Range-Time Representation 23

3.5 Achievable SNR as a function of τ, R 25

4.1 Ground-Clutter Geometry 32

4.2 E-Region Magnetic-Aspect Contours from a Satellite-Borne Radar (h = 400 km) 36

4.3 Maximum Ground-Clutter Range Dependence on Spacecraft Altitude 39

4.4 Representative Ionospheric and Ground-Clutter Radar Signal Returns 39

4.5 Frequency Power Spectrum as a Function of f, τ 41

4.6 Artist's Drawing of 600-ft Unfurled Antenna and Space Shuttle 50

4.7 Drag Force as a Function of Antenna Diameter and Spacecraft Altitude 53

4.8 Spacecraft Altitude Decrease as a Function of Time and Antenna Diameter 55

4.9 SNR Dependence on λ, τ for a Fixed-Dimension Phased-Array Antenna 63

TABLES

3.1 Waveform Characteristics 21

4.1 Power Aperture Requirements, Given Energy-Storage Capabilities, and Radar Waveforms. 48

PRECEDING PAGE BLANK NOT FILMED

1. INTRODUCTION

The development of the incoherent-scatter radar into a powerful ground-based remote sensor of ionospheric plasma parameters is now well known.[1*] Its impact on the understanding of auroral and magnetospheric processes has been clearly demonstrated with the installation and operation of the Chatanika incoherent-scatter radar.[2] Therefore, it is only natural that such a radar be considered as an experiment in the AMPS (Atmospheric, Magnetospheric and Plasmas in Space) program on board the Space Shuttle.

The Satellite-borne incoherent-scatter radar will be capable of making ionospheric measurements on a global scale covering regions of interest from the equator to the polar cap. Measurements could be made to complement other plasma measurements[3] to be conducted on Space Shuttle. Its remote-sensing capability is particularly attractive as a means of making plasma-parameter measurements in the vicinity of subsatellite experiments that are being considered using a mother-daughter configuration.[4]

To examine the feasibility of an incoherent-scatter radar aboard Space Shuttle, we begin in Section 2 by estimating the signal-to-noise ratio (SNR). Since SNR is the critical parameter, we present its calculations in detail. We show that due to the competing frequency dependence of the cosmic noise power and the spectral width associated with the incoherent-scatter signal, SNR is optimized in the frequency range from 300 to 1000 MHz.

In Section 3, we examine the factors that affect the selection of an appropriate waveform for incoherent-scatter experiments--in particular,

---

*References are listed at the end of the report.

SNR, range resolution, and frequency resolution. We propose two possible waveforms for use aboard Space Shuttle--a single 200-μs pulse, and a five-pulse burst of 20-μs pulses. Then, using the SNR equations derived in Section 2 together with the proposed waveforms, we consider the tradeoffs and constraints placed on a satellite-borne incoherent-scatter radar. The major problem areas are: (1) limited available power, (2) the presence of ground clutter and field-aligned clutter, (3) the transmitter and antenna design to achieve the required SNRs, and (4) the effects of orbital motion on averaging time and spatial resolution.

In the process of considering the incoherent-scatter radar parameters, we find that the same radar could also be used in a semicoherent backscatter mode to map the field-aligned electron-density irregularities found in the auroral and polar cap regions. We briefly examine the scientific benefits of such an experiment in Section 5.

2. SIGNAL-TO-NOISE-RATIO ESTIMATION

The parameter of greatest importance in evaluating the feasibility of an incoherent-scatter radar aboard the Space Shuttle is the expected SNR. Since the SNR is so critical, and since some approximations must be made to estimate it, the calculation of the SNR is described in detail in this section.

2.1 Signal Power

The calculation of expected signal power begins with the general radar equation:

$$P_r = \left(\frac{P_t G_t}{4\pi R^2}\right)\frac{\sigma A}{4\pi R^2} \tag{2.1}$$

where

P_r = Received power (watts)

P_t = Transmitted power (watts)

G_t = Gain of transmitting antenna

R = Range to target (m)

σ = Radar cross section of target (m^2)

A = Effective aperture of receiving antenna (m^2).

The term $\left(P_t G_t/4\pi R^2\right)$ represents the power density (W/m^2) at the target. This quantity times σ represents the power intercepted by the target and reradiated toward the receiver. Then $P_t G_t \sigma/(4\pi R^2)^2$ is the power density (W/m^2) at the receiver. Finally, the antenna of effective aperture A collects the power (P_r) given by Eq. (2.1).

For a distributed target, such as the ionosphere, the radar cross section is made up of the sum of the cross sections of a large number of scatterers contained within the volume being probed.

$$\sigma = \sigma_o N' V \tag{2.2}$$

where

σ_o = Equivalent radar cross section of a single scatterer (m^2)

N' = Number of scatterers per unit volume (m^{-3})

V = Volume probed by the radar (m^3).

For the incoherent-scatter "ionic" component,[1] σ_o is given by

$$\sigma_o = \frac{4\pi(r_e \sin \varphi)^2}{(1+\alpha^2)(1+T_e/T_i+\alpha^2)} \tag{2.3}$$

for $T_e/T_i < 4$

and $\alpha^2 < 1$

where

r_e = Classical electron radius (2.82×10^{-15} m)

φ = Angle between the direction of the incidence electric field and the direction to the observer

= $\pi/2$ for backscatter case

T_e = Electron temperature (°K)

T_i = Ion temperature (°K)

N = Electron density (el/m^3)

D = $69\ (T_e/N)^{1/2}$ = electron Debye length (m)

λ = Radar wavelength (m)

α^2 = $(4\pi D/\lambda)^2$.

For typical ionospheric parameters and operating wavelengths, the denominator of Eq. (2.3) is about 3, and the numerator (for the backscatter

case) is 10^{-28} m^2. Thus,

$$\sigma_o \approx 3 \times 10^{-29} \ m^2 \quad . \tag{2.4}$$

In the case of a pulsed monostatic radar system, the scattering volume, V, is determined by the transmitted pulsewidth, τ, and the beamwidth of the radar antenna, θ_B. The beamwidth in one dimension is given approximately by

$$\theta_B \approx \frac{\lambda}{a} \quad \text{(radians)} \tag{2.5}$$

where a = physical linear dimension of the antenna (m). Using $\theta_B R$ as the linear dimension orthogonal to the beam direction, the cross-sectional area of the volume is

$$\text{Area} \approx \theta_B^2 R^2 = \frac{\lambda^2}{a^2} R^2 \quad . \tag{2.6}$$

But the physical area of a square antenna, A_o, is a^2 and the effective collecting area for typical antennas is $A \approx A_o/2$. Thus, the cross-sectional area of the volume being probed is

$$\text{Area} \approx \frac{\lambda^2}{A_o} R^2 \approx \frac{\lambda^2 R^2}{2A} \quad . \tag{2.7}$$

Therefore, the volume probed is this area times one-half the length in space of the transmitted pulse:

$$V = \text{Area} \cdot \frac{c\tau}{2}$$

$$= \frac{\lambda^2 R^2}{2A} \frac{c\tau}{2} = \frac{\lambda^2 R^2 c\tau}{4A} \quad . \tag{2.8}$$

Using Eqs. (2.2) and (2.8), and the relationship between antenna gain and effective aperture

$$G = \frac{4\pi A}{\lambda^2} \tag{2.9}$$

we can substitute Eqs. (2.8) and (2.9) in Eq. (2.1) to obtain

$$P_r = P_t \left(\frac{4\pi A}{\lambda^2}\right) \frac{1}{4\pi R^2} \sigma_o \frac{N\lambda^2 R^2 c\tau}{4A} \frac{A}{4\pi R^2}$$

$$= \frac{P_t \sigma_o N c \tau A}{16\pi R^2}$$

$$= \left(\frac{c\sigma_o}{16\pi}\right)\left(\frac{P_t A \tau N}{R^2}\right) \tag{2.10}$$

Note that we have substituted the electron (number) density, N, for N′. Numerically evaluating the constants, we find

$$P_r \approx 2 \times 10^{-22} \frac{P_t A \tau N}{R^2} \quad \text{(watts)} \tag{2.11}$$

Thus we see that the received signal power is directly proportional to the transmitted power, the effective antenna aperture, and the electron density, and inversely proportional to the square of the range to the scattering volume. This relationship is applicable only to a monostatic pulsed radar. Further it applies only to the power contained within the ionic part of the incoherent-scatter spectrum.

2.2 Noise-Power Calculation

2.2.1 System Noise Temperature

The radar system noise level contains contributions from the receiver itself, contributions due to losses in the RF portion of the receiving system, and contributions from the sky (or ground) background.

Figure 2.1 shows (1) the maximum and minimum temperatures due to cosmic noise, (2) the maximum temperature that would be seen if the antenna were viewing the earth, and (3) a typical receiving system temperature (including losses).

If the antenna is pointed toward the earth (i.e., "earth-oriented" sector), we can expect a system temperature, independent of frequency, of about 400°K, the sum of the receiver temperature plus the earth temperature.

If the antenna is pointed away from the earth (i.e., "space-oriented" sector), the system temperature is dependent on (1) where in the galactic sphere the antenna is pointed, and (2) what radio frequency is used. For the purposes of this calculation, we will use the following expression for the cosmic noise temperature:

$$T_c = \left(\frac{300}{f}\right)^{2.34} = 100\ \lambda^{2.34} \tag{2.12}$$

where

f = Operating frequency (MHz)

λ = Wavelength (m).

This mean cosmic-noise temperature is shown in Figure 2.1 by the sloping dashed line. Thus, the total system temperature in the space-oriented sector will be the sum of T_c and the receiving system temperature,

$$T_s = 100\ (1 + \lambda^{2.34}) \quad . \tag{2.13}$$

2.2.2 Bandwidth Requirements

The required operating bandwidth is determined by the width of the ionic component of the incoherent-scatter spectrum, and/or the equivalent spectral width of the transmitted pulse. The half-power (center frequency to half-power point) spectral width of the incoherent-scatter

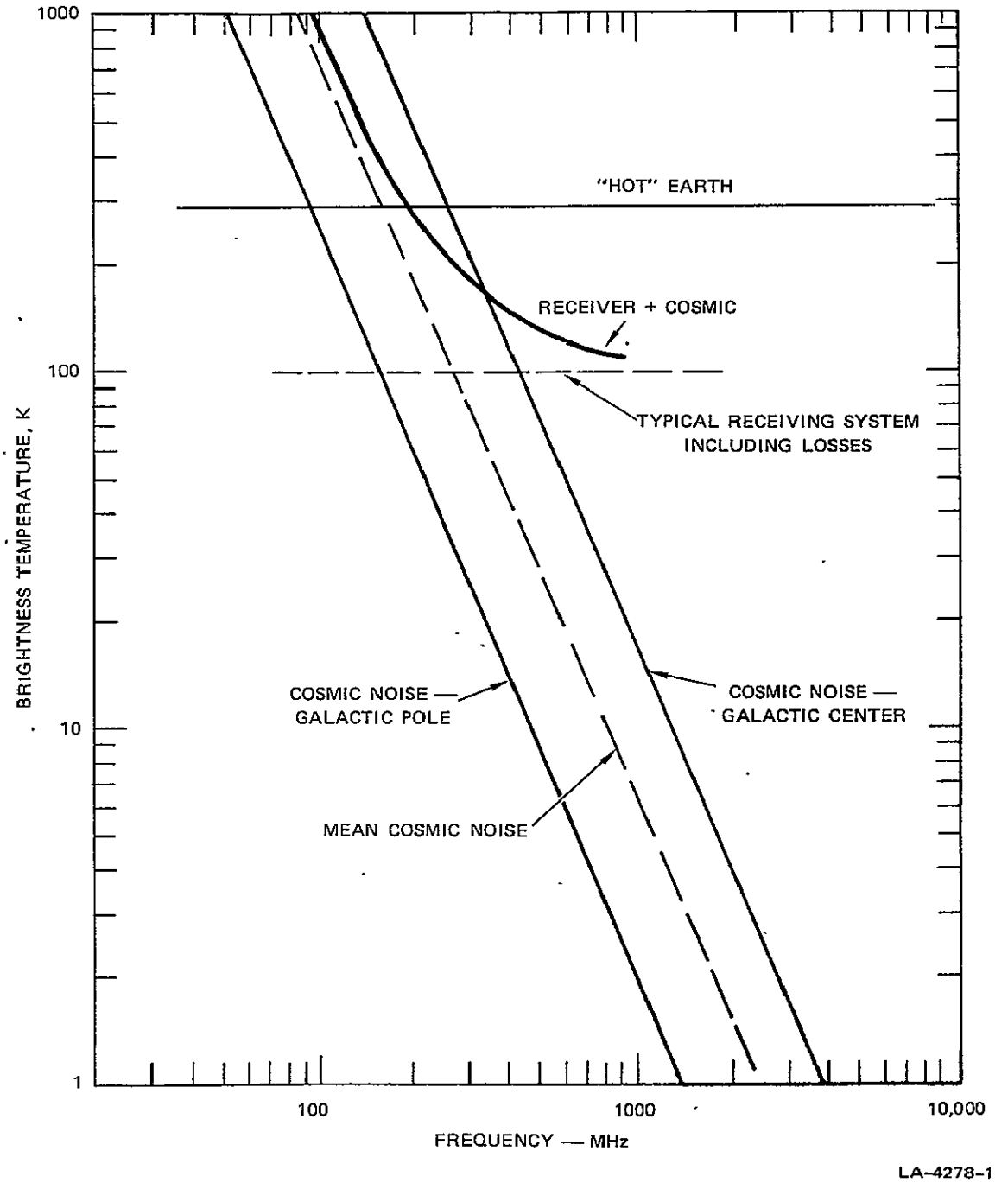

FIGURE 2.1 COSMIC NOISE AND RECEIVER TEMPERATURES vs FREQUENCY

ORIGINAL PAGE IS
OF POOR QUALITY

signal is approximately 1.5 times the Doppler shift expected for an ion approaching at the mean thermal speed of the ions,[1] $(2KT_i/m_i)^{1/2}$. A wider measurement bandwidth must be used to include all of the spectrum on both sides of center frequency. The total bandwidth necessary to pass all the signal power is about

$$\Delta f_i \approx \frac{8}{\lambda}\left(\frac{2KT_i}{m_i}\right)^{1/2} \quad \text{(Hz)} \tag{2.14}$$

where

$K = 1.38 \times 10^{-23}$ joules/°K Boltzmann's constant

T_i = Ion temperature (°K)

m_i = Ion mass (kg).

As an upper bound, we use 1500°K for the temperature of O^+ ions. Substituting that value in Eq. (2.14) gives

$$\Delta f_i = \frac{10^4}{\lambda} \quad \text{(Hz)} \quad . \tag{2.15}$$

This would be the required bandwidth if there were no (or very small) Doppler shift of the signal due to the relative motion between the radar and the plasma under study, or if the mean Doppler shift were reduced to near zero by adjusting the receiver local oscillator.

The bandwidth necessary to pass a pulse of width τ is

$$\Delta f_\tau \approx \frac{1}{\tau} \quad \text{(Hz)} \quad . \tag{2.16}$$

Thus the total required receiver bandwidth may be estimated from the following equation:

$$\Delta f = \Delta f_i + \Delta f_\tau = \frac{10^4}{\lambda} + \frac{1}{\tau} \quad \text{(Hz)} \quad . \tag{2.17}$$

Note that by using Eq. (2.17) as the required bandwidth, we may overestimate the actual bandwidth by no more than a factor of two.

2.2.3 Total Noise Power

The total noise power is estimated by

$$P_n = K T_s \Delta f \quad . \tag{2.18}$$

Substituting the expressions for T_s (for the space-oriented sector) and Δf [Eqs. (2.13 and (2.17)] in Eq. (2.18), we find

$$P_n = 1.38 \times 10^{-21}\left[1 + \lambda^{2.34}\right]\left[\frac{10^4}{\lambda} + \frac{1}{\tau}\right] \quad . \tag{2.19}$$

The noise power as a function of wavelength (frequency) for several values of pulsewidth is plotted in Figure 2.2. When the antenna is pointed in the space-oriented sector and when long pulsewidths (hundreds of microseconds) are used, the noise power is minimum around 300 to 400 MHz and is not strongly frequency-dependent between 200 and 800 MHz. For short pulsewidths (<100 μs), the noise power is increased at all frequencies and increases rapidly as the frequency is lowered below about 400 MHz.

In calculating the space-oriented-sector curves of Figure 2.2, the mean cosmic-noise curve in Figure 2.1 [or Eq. (2.12)] was used. The noise power at frequencies below about 400 MHz could easily be decreased or increased by as much as a factor of 2.

When the antenna is pointed toward the earth, the noise power is greater than that in the space-oriented sector at all frequencies above 200 MHz, and is less than that in the space-oriented sector for frequencies less than 200 MHz.

2.3 Signal-to-Noise Ratio

The signal-to-noise ratio is defined by

$$SNR \equiv P_r/P_n \quad . \tag{2.20}$$

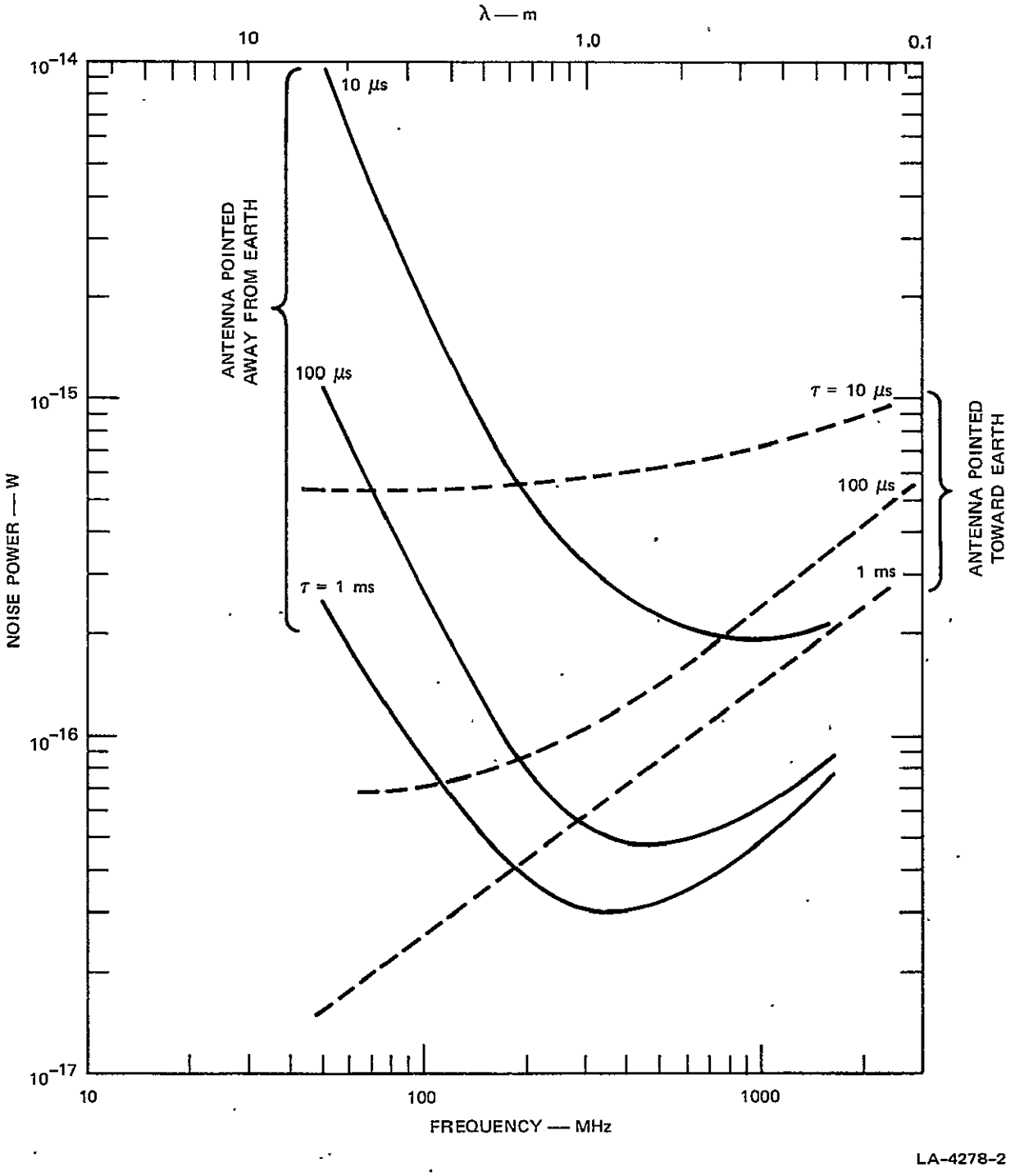

FIGURE 2.2 TOTAL NOISE POWER vs FREQUENCY

For directions away from earth, we obtain from Eqs. (2.11) and (2.19)

$$\mathrm{SNR} = \frac{0.145(P_t A)\, N \tau}{R^2\left[1 + \lambda^{2.34}\right]\left[10^4/\lambda + 1/\tau\right]} \tag{2.21}$$

For directions toward the earth, we obtain from Eqs. (2.11) and (2.18) [with $T_s = 400°K$]

$$\mathrm{SNR} = \frac{0.037(P_t A)\, N \tau}{R^2\left[10^4/\lambda + 1/\tau\right]} \quad . \tag{2.22}$$

2.3.1 λ, τ Dependence

Let us first investigate the dependence of SNR on wavelength and pulse length. Equations (2.21) and (2.22) have been plotted in Figure 2.3. SNRs for the space-oriented sector are plotted as solid curves and those for the earth-oriented sector as dashed curves.

For directions toward the earth, the SNR decreases with increasing frequency due to the increased receiver bandwidth requirement at higher frequencies. When long pulsewidths are used, i.e., when $\tau \gg \lambda/10^4$ [see Eq. (2.22)], the SNR varies inversely with frequency since the bandwidth, and thus the noise power, increases linearly with frequency. For short pulsewidths, i.e., $\tau \ll \lambda/10^4$, the SNR is almost constant, since the required bandwidth is determined by the fixed transmitted pulse spectrum and not the signal spectrum.

For directions away from earth, the SNR maximizes at a particular frequency for a given pulsewidth. At lower frequencies, the SNR decreases due to the increased cosmic-noise temperature. At higher frequencies the SNR decreases due to the increased bandwidths required to pass the signal spectrum. As the pulsewidth is shortened, the maximum SNR moves to higher frequencies. For the pulsewidths likely to be of

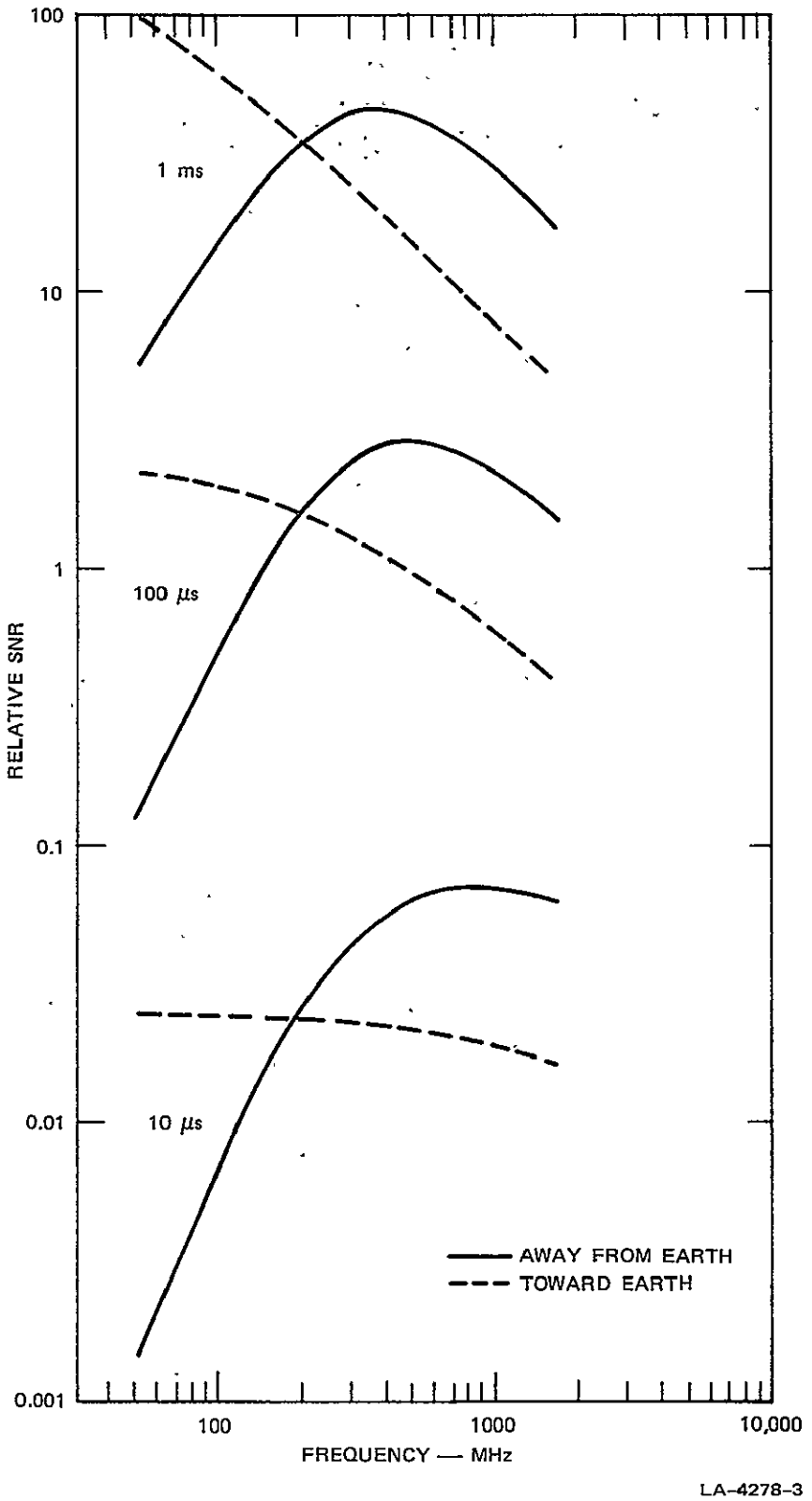

FIGURE 2.3 SNR DEPENDENCE ON λ, τ

ORIGINAL PAGE IS
OF POOR QUALITY

use on the Space Shuttle (20 to 200 μs)--see Section 3--frequencies between 300 and 1000 MHz are optimum.

2.3.2 Power-Aperture Requirement

Next, we investigate the power-aperture product necessary to give usable SNRs. In the calculations for this section, we make the following assumptions:

(1) $\lambda = 0.5$ m (600 MHz). From Section 2.3.1, we saw that for pulsewidths in the range 20 to 200 μs, the optimum frequency was between 300 and 1000 MHz.

(2) An SNR = 0.1 is required at a range, R, of 100 km for an electron density, N, of 10^{11} el/m^3.

Then we solve the following equations [derived from Eqs. (2.21) and (2.22)] for the product P_tA as a function of pulsewidth:

Space-oriented Sector

$$P_tA = \frac{0.1 \times (10^5)^2 \times 1.2 \times (2 \times 10^4 + 1/\tau)}{0.145 \times 10^{11} \times \tau}$$

$$= \frac{0.083}{\tau} (2 \times 10^4 + 1/\tau) \qquad (2.23)$$

Earth-oriented Sector

$$P_tA = \frac{0.1 \times (10^5)^2 \times (2 \times 10^4 + 1/\tau)}{0.037 \times 10^{11} \times \tau}$$

$$= \frac{0.27}{\tau} (2 \times 10^4 + 1/\tau) \quad . \qquad (2.24)$$

The results are shown in Figure 2.4. For a wavelength of 0.5 m, a range of 100 km, an electron density of 10^{11} el/m^3, and a required SNR of 0.1, a total range of power-aperture products between 10^7 and 10^9 is needed to

ORIGINAL PAGE IS
OF POOR QUALITY

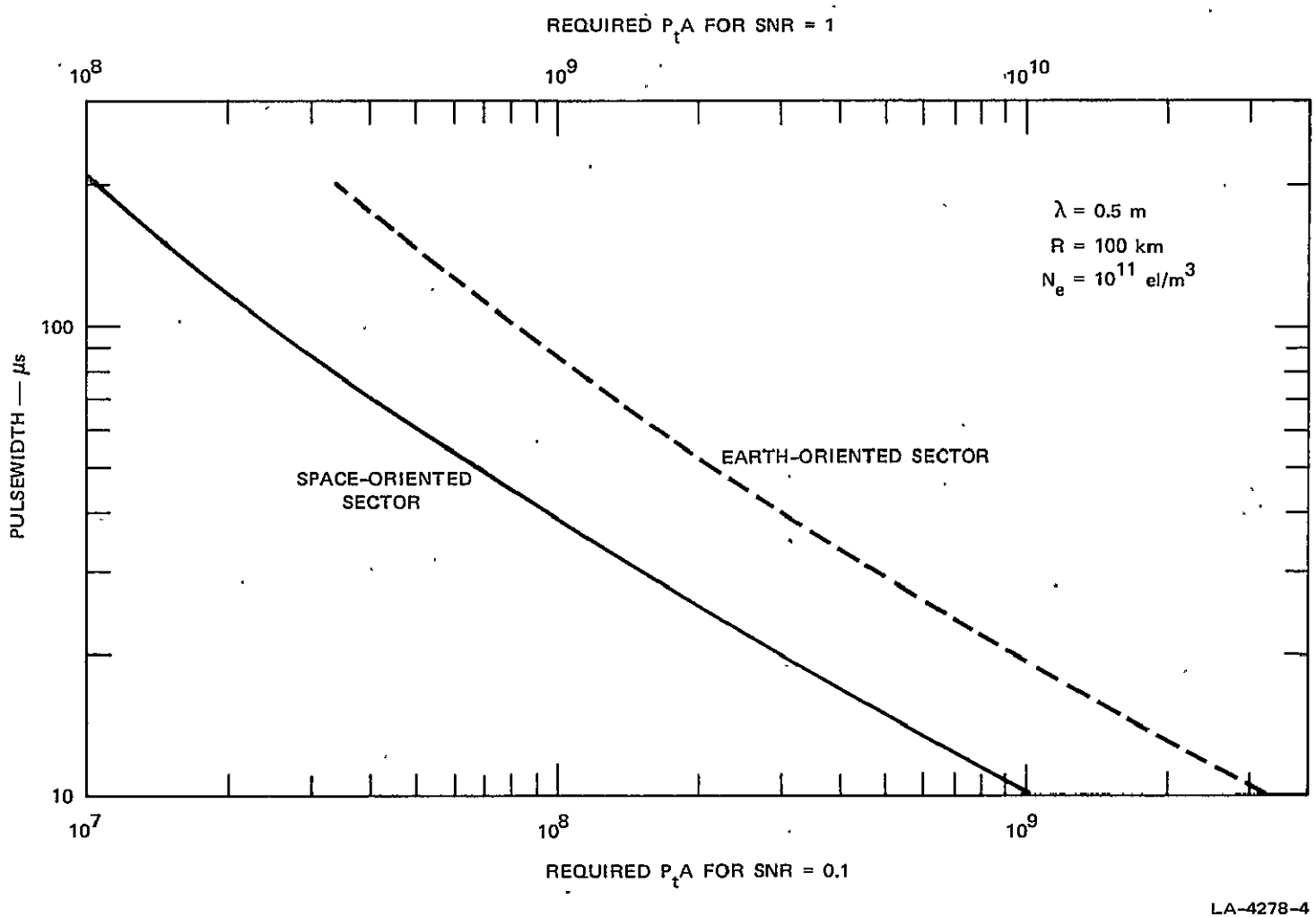

FIGURE 2.4 POWER-APERTURE-PRODUCT REQUIREMENT

cover the pulsewidths of interest with any radar viewing angle. In the space-oriented sector, the range of power-aperture products is reduced to between 10^7 and 2×10^8. In the earth-oriented sector, the range is between 3.5×10^7 and 10^9. Alternatively, for a given pulsewidth, the range of power-aperture products is even more limited. For example, for a 20-μs pulsewidth, the range is between 2×10^8 and 10^9. Since the SNR is directly proportional to P_tA, the numbers obtained for an SNR = 0.1 can be directly scaled to any other desired SNR. For convenience, the required P_tA for an SNR = 1.0 is given at the top of Figure 2.4.

To get an idea of the implications of the calculated power-aperture product requirement, let us assume that an operating mode (pulsewidth) is chosen such that the required P_tA is 10^8. A Lockheed study of unfurlable antennas states that it is now possible to design unfurlable reflectors as large as 600 ft (183 m) in diameter to operate at 500 MHz. They further predict that antennas of these sizes operating at 6 to 10 GHz will be available by 1985. If we assume a physical circular aperture 183 m in diameter, then the effective aperture will be approximately 1.3×10^4 m^2. If an antenna of this area were flown on the AMPS Space Shuttle, then a peak power of about 10 kW would be required. A more detailed discussion of power-aperture products is given in Section 4.

3. WAVEFORM DESIGN

3.1 General

Several factors influence the design of an appropriate waveform for incoherent-scatter experiments. The most important of these are:

(1) Signal-to-noise ratio: As was discussed in the previous section, the longer the pulsewidth, the greater the signal-to-noise ratio. In some regions ($\tau \ll \lambda/10^4$) the SNR improves as the square of the pulsewidth [see Eqs. (2.21) and (2.22)].

(2) Maximum range of interest: This factor is related to Item 1 in that improved SNRs will allow probing to greater ranges.

(3) Range resolution: The range resolution is directly proportional to the pulsewidth. Better range resolution requires shorter pulses, which in turn reduce the SNR and the maximum range.

(4) Lag (or frequency) resolution: In order to estimate plasma temperatures and velocity, the autocorrelation function (ACF) or the spectrum of the signal must be computed from the radar measurements. The ACF must be computed at time lags short enough and spaced closely enough to adequately characterize the shape of the ACF, and for lags long enough to encompass at least the second zero-crossing of the ACF.

The required lag resolution and maximum lag are functions of the plasma parameters. We desire to find a waveform (or a small set of waveforms) that provides the required lag resolution over the range of plasma parameters that can be expected to occur. Figures 3.1 and 3.2 show theoretical spectra and ACFs for a range of typical plasma parameters. These figures are applicable to an operating frequency of 600 MHz, but can be easily scaled for other frequencies.

In Figure 3.1, the ratio of electron to ion temperature (T_e/T_i) is varied from unity to 3.5, with the ion temperature fixed at 800°K. In Figure 3.2 the temperature ratio is held fixed at unity while the ion (and electron) temperatures are varied between 400°K and 1600°K. From these figures, we see that the ACF needs to be measured to a maximum lag of about 200 μs, and that a lag resolution of 20 μs would be adequate.

The simplest waveform that could be used is a single pulse transmitted at regular intervals. The shorter the pulse, the better the range resolution but the worse the frequency resolution and the SNR. When the frequency- and range-resolution requirements are incompatible, (i.e., when the spectral width of the transmitted pulse exceeds the spectral width of the scattered signal), then single-pulse transmissions cannot be used.

Waveforms containing sequences of two or more appropriately spaced short pulses have range resolution corresponding to the short individual pulses and frequency resolution corresponding to the overall length of the pulse sequence. This multiple-pulse method yields satisfactory range and spectral resolution at the expense of the SNR. The SNR is reduced not only because of the shortness of the pulse and the corresponding wide receiver bandwidths but also because of clutter (signals from unwanted altitudes), which adds to the noise.

Clutter can be reduced by transmitting at more than one frequency and/or by using orthogonal polarizations. However, Farley[6] has shown that efforts to eliminate clutter are usually not worthwhile, and the optimum procedure in most cases is to transmit a sequence of several suitably spaced pulses. Such a procedure generally makes more efficient use of the average-power capabilities of the transmitter than do other techniques. This is a very important consideration for the Space Shuttle.

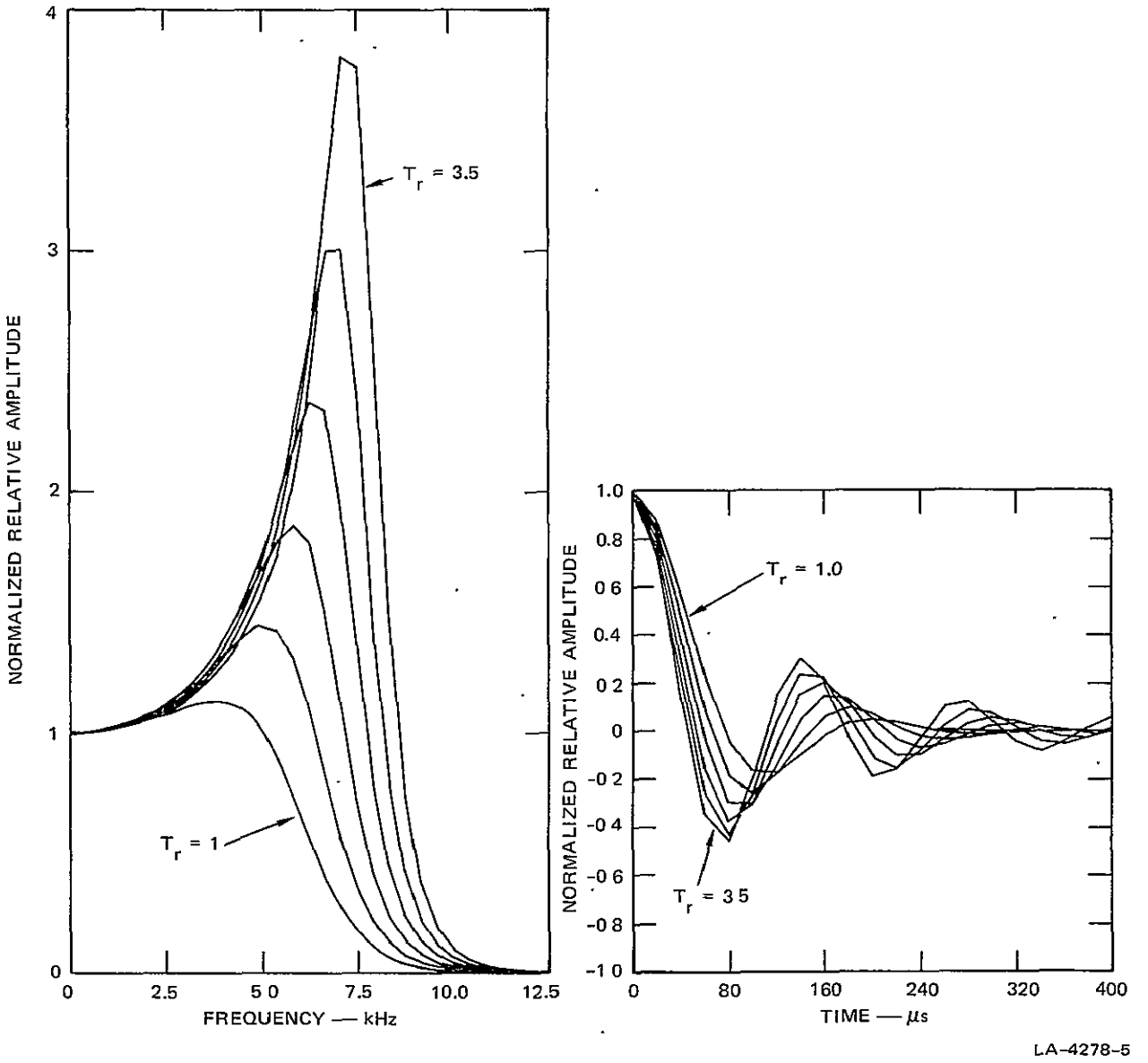

FIGURE 3.1 THE T_r VARIATION OF THE POWER SPECTRA AND AUTOCORRELATION FUNCTIONS (ACFs)

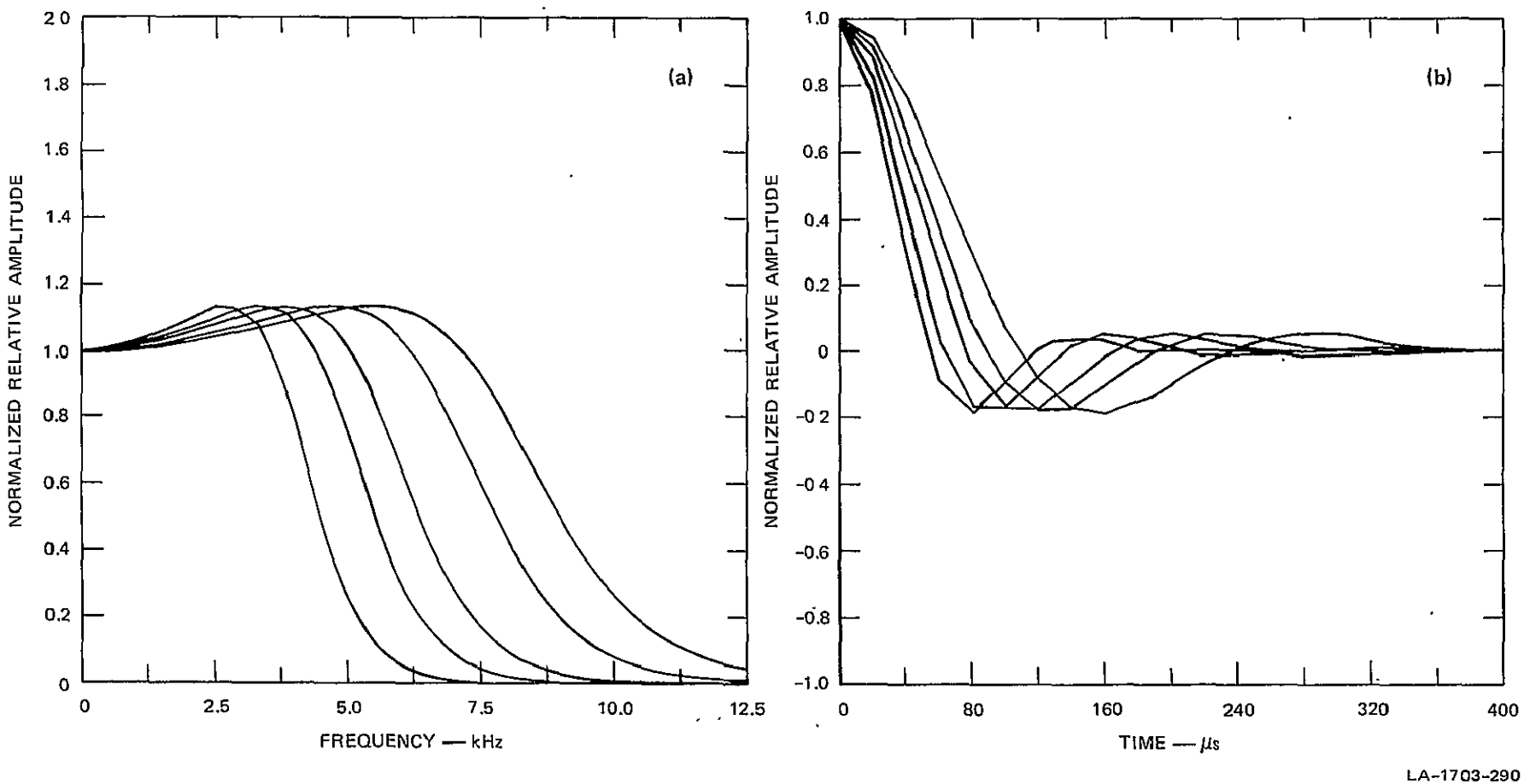

FIGURE 3.2 THE T_i VARIATION OF THE POWER SPECTRA AND ACFs

3.2 Two Possible Waveforms

We next postulate two waveforms for possible use abroad the Space Shuttle. Both waveforms have about the same frequency resolution; however the range resolutions offered are an order of magnitude different, as are the expected SNRs. The waveforms considered are:

(1) A single pulse 200 μs long.

(2) A five-pulse burst of 20-μs pulses. The burst extends over 240 μs of time. Enmeshed in the burst is a single 20-μs pulse transmitted at a frequency displaced by a megahertz or so from the frequency of the five-pulse burst. The displaced frequency pulse is needed to measure the zero-lag autocorrelation coefficient and hence the signal power as a function of range.

The pertinent characteristics of the two waveforms are given in Table 3.1, and range-time diagrams for each waveform are shown in Figures 3.3 and 3.4, respectively.

Table 3.1

WAVEFORM CHARACTERISTICS

	Waveform 1	Waveform 2
Number of pulses	1	6 (5 at f_1, 1 at f_2)
Length of individual pulse, μs	200	20
Length of waveform, μs	200	240
Range resolution, km	30	3
Lag resolution, μs	20	20
Frequency resolution, kHz	~5	~4
Minimum range, km	~40	~40
Relative energy transmitted per waveform	1	0.6

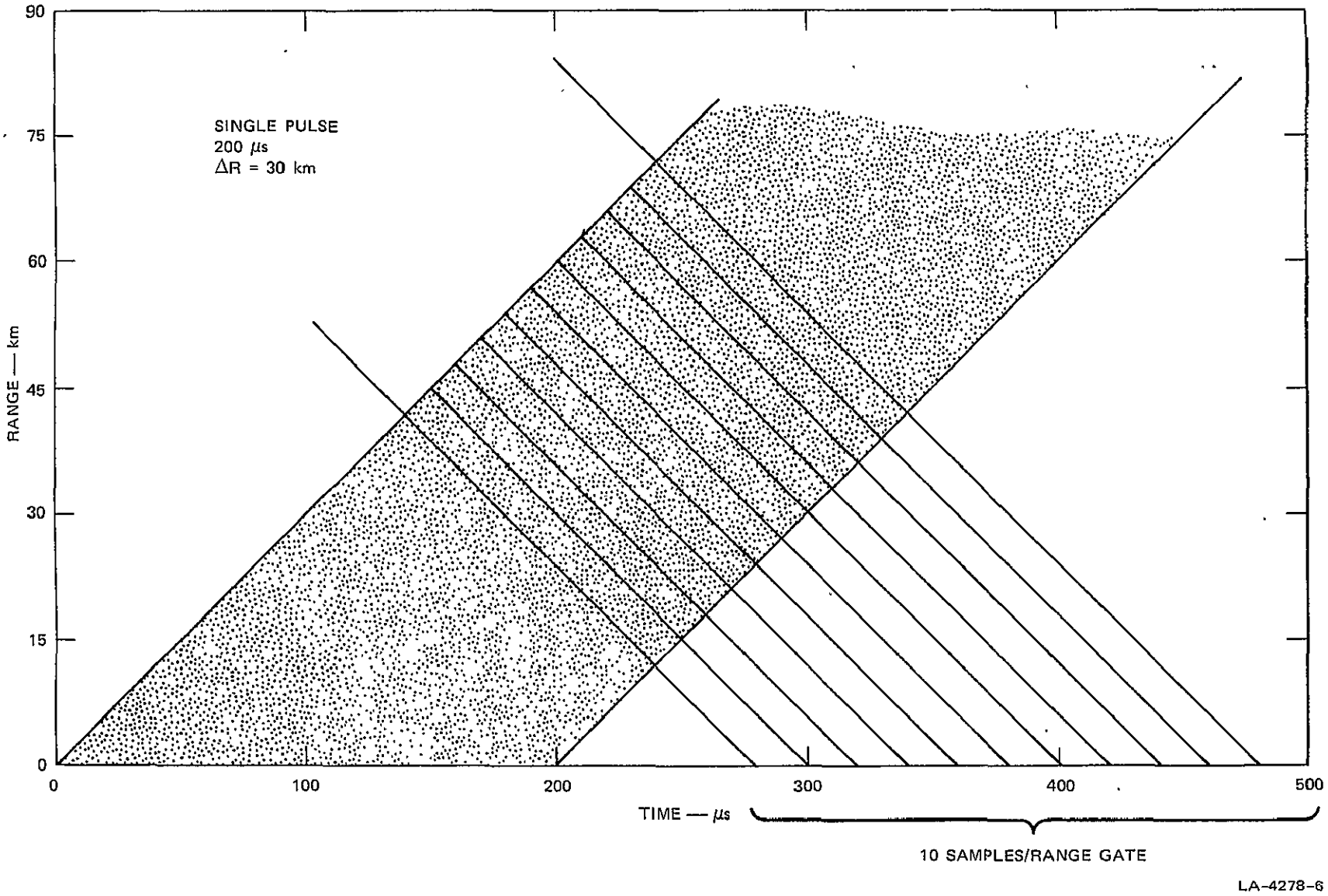

FIGURE 3.3 SINGLE-PULSE RANGE-TIME REPRESENTATION

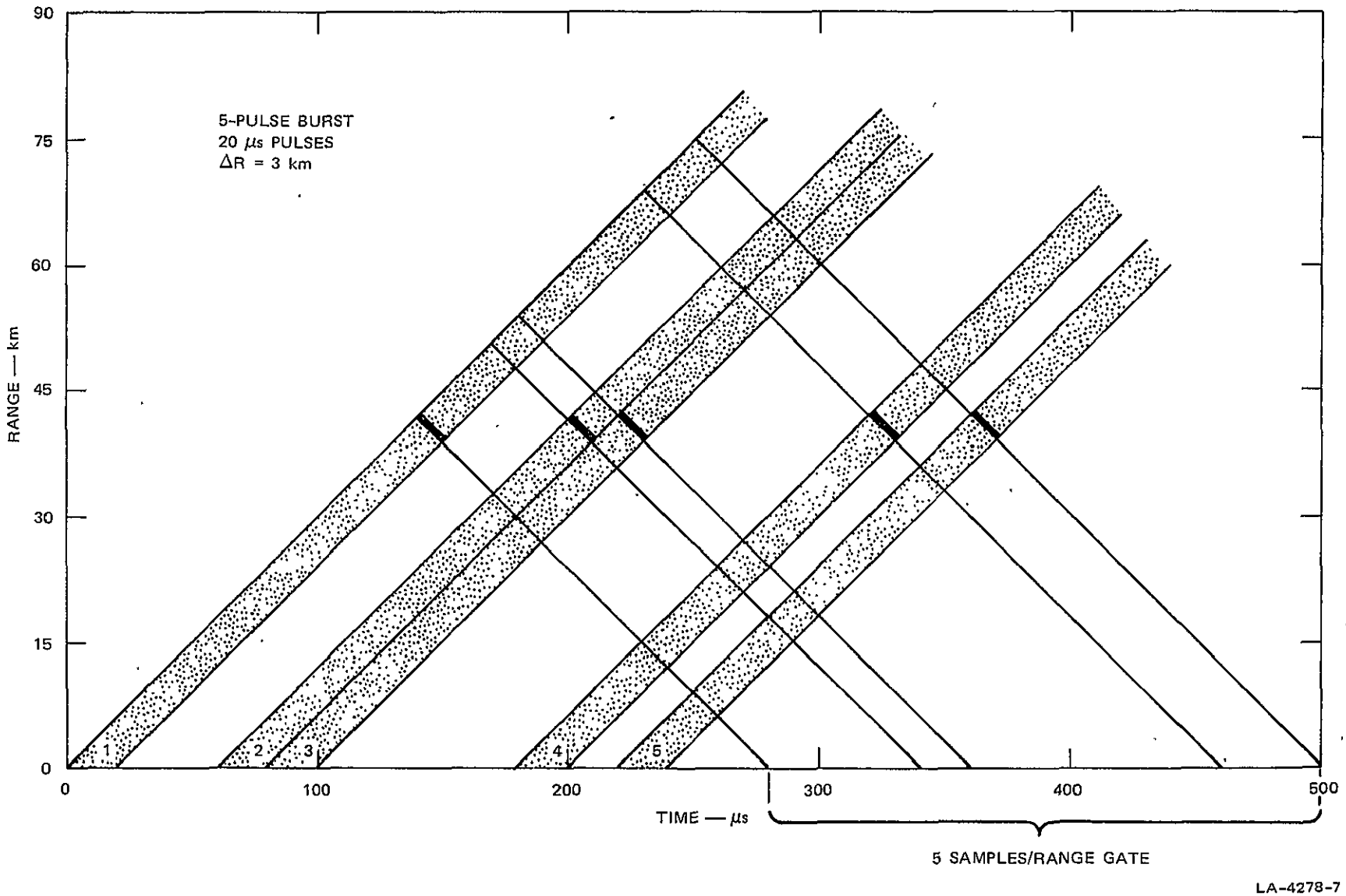

FIGURE 3.4 PULSE-BURST RANGE-TIME REPRESENTATION

For the two waveforms described above, we can calculate the expected SNR as a function of range using the following assumptions:

$\lambda = 0.5$ m

$P_t = 10^4$ watts

$N = 10^{11}$ el/m^3

$A = 1.3 \times 10^4/m^2$ (183 m reflector).

The results are shown in Figure 3.5. For a 200-μs pulse, usable SNRs (~ 0.1) are achieved to ranges of a few hundred kilometers. The radar sensitivity could be reduced by an order of magnitude (200-ft antenna, or 1 kW of peak power) and reasonable SNRs would be maintained to at least 100 km range.

For the 20-μs, five-pulse burst waveform, the SNRs are marginal at ranges greater than 70 km in the space-oriented sector, and at essentially all ranges in the earth-oriented sector for the assumed system sensitivity. Reasonable SNRs would be obtained to 100 km only for electron densities in excess of about 3×10^{11} el/m^3 (three times bigger than used in the calculation of Figure 3.5). We note that the self-clutter due to the burst waveform has not been included in the calculations.

The SNR for the multipulse waveform can be improved by a factor of 1.67 if one constrains the average power to be 10^3 watts and allows the peak power to be increased by the ratio of 200/120 (i.e., 16.67 kW instead of 10 kW), so that the energy transmitted in each of the two waveforms is equal.

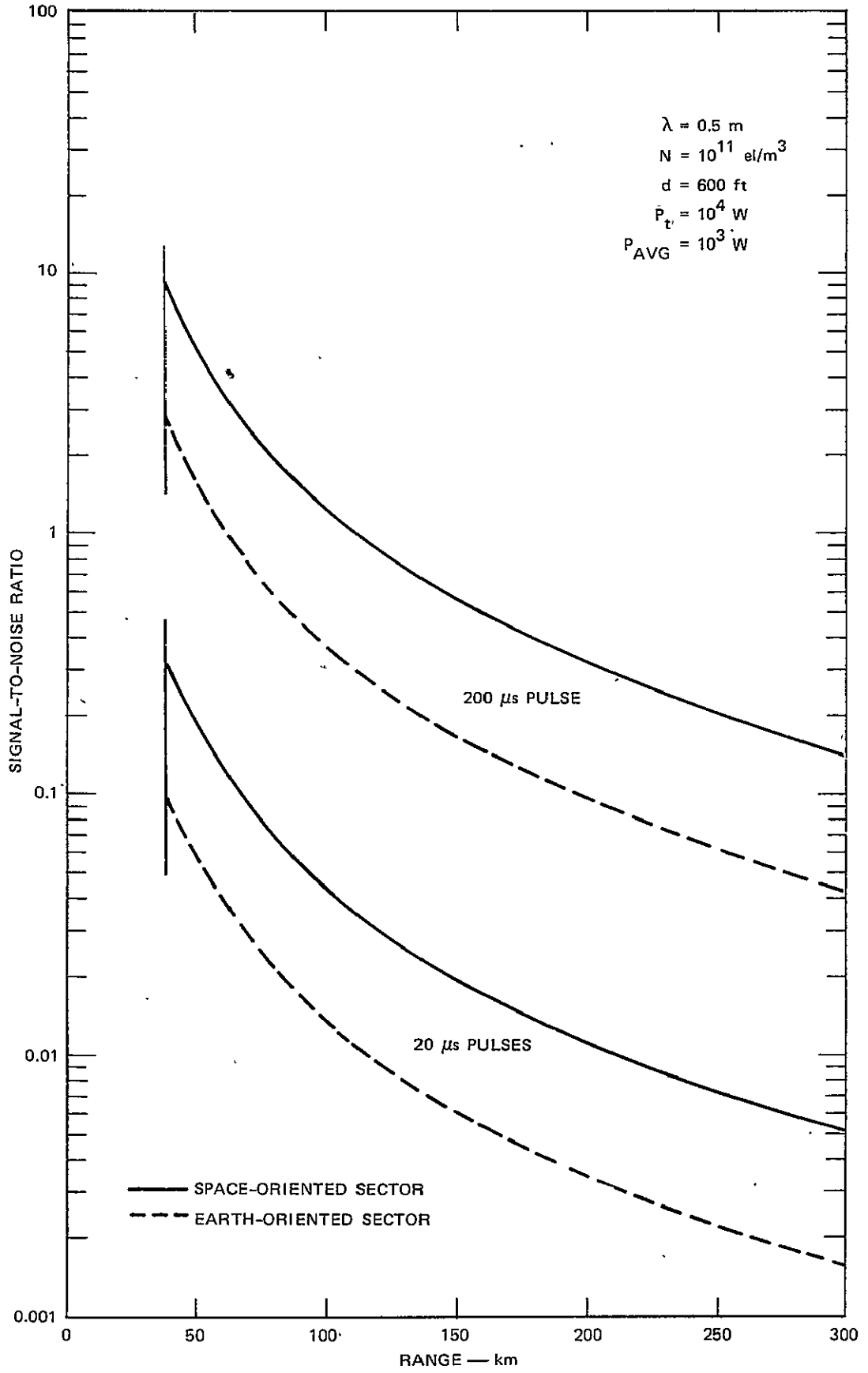

FIGURE 3.5 ACHIEVABLE SNR AS A FUNCTION OF τ, R

ORIGINAL PAGE IS
OF POOR QUALITY

4. TRADEOFFS AND CONSTRAINTS

In designing an incoherent-scatter radar for the Space Shuttle, many tradeoffs are possible. Also, constraints imposed by the Shuttle will heavily influence the design. In this section we examine some of the constraints and tradeoffs, including:

(1) Utilization of available power. Given that the available average power is limited, how should that power be used; is it better to generate high-peak-power pulses at a slow repetition rate or lower peak powers at a higher repetition rate?

(2) Clutter. What are the limitations imposed by ground (and auroral) clutter on the design of the radar--e.g., choice of waveform repetition frequency? Is clutter mitigation feasible?

(3) Averaging times versus spatial resolution. What are the tradeoffs between averaging time and spatial resolution; how few pulses can be used to derive meaningful averages?

(4) Transmitter. What are the implications of the peak power, average power, and repetition rates on the transmitter design and efficiency; what would the overall efficiency of the transmitter be (including conversion of prime power from 28 Vdc to whatever the transmitter needs); what would be the weight and volume of typical transmitters?

(5) Antenna. How big an antenna is possible; what would be the weight and volume of the antenna; how (and how rapidly) could it be steered; and would the drag of such an antenna significantly perturb the Shuttle orbit? For the peak transmitter powers being considered, is antenna breakdown due to gas discharge important? If so, can its effects be circumvented by proper antenna design?

PRECEDING PAGE BLANK NOT FILMED

4.1 Utilization of Available Power

Aboard the Space Shuttle, an incoherent-scatter radar will be average-power limited. We must therefore consider what constraints this places on the radar parameters such as peak transmitted power and waveform repetition rate. In Section 2, the importance of SNR was discussed and applicable formulas were developed that involved the peak pulsed power. SNR is, however, not the only parameter that must be accounted for in order to make accurate incoherent-scatter measurements. Since the incoherent-scatter signal is produced by a random ensemble of scatterers, a certain amount of averaging must be employed, regardless of the SNR, to accurately measure its mean characteristics. This is true even for SNRs well in excess of unity.

In order to determine the most efficient use of the available power, we must consider the factors that affect the variance of the averaged quantity. The standard deviation, σ, of the incoherent-scatter measurement of most ionospheric parameters varies approximately as

$$\sigma \propto \left[C + \left(\frac{1}{\mathrm{SNR}}\right)\right] \frac{1}{\sqrt{n}} \tag{4.1}$$

where C is a constant of the order of unity, and n is the number of samples used in the averaging. When the SNR is very small, σ is large but decreases in proportion to increases in SNR. When the SNR approaches 1/C, further increases in SNR decrease σ by only a small amount. To summarize, we see from Eq. (4.1) that it is desirable to increase the SNR only until it is of the order of 1/C, then one should work toward increasing n.

How does this influence the selection of the transmitted power? In the small-SNR case, a measure of the system, S, is

$$S \equiv \frac{1}{\sigma} \approx \mathrm{SNR}\sqrt{n} \quad . \tag{4.2}$$

For fixed parameters (N, A, R), we see from Eq. (2.22) that

$$S \approx \frac{C_1 P_t \tau}{(10^4/\lambda + 1/\tau)} \sqrt{\frac{t_m}{t_p}} \tag{4.3}$$

where

C_1 = Constant

$n = t_m/t_p$

t_m = Total measurement (integration) time

t_p = Waveform repetition interval.

But the peak transmitted power P_t is related to the average power $\overline{P}$ by

$$P_t = \frac{\overline{P} t_p}{t_{ON}} \tag{4.4}$$

where t_{ON} is the total time the transmitter is turned on during the waveform repetition interval t_p (i.e., t_{ON}/t_p is the duty cycle of the transmitter). From Eq. (4.3), it is clear that the system sensitivity is improved by increasing the peak transmitted power. However, since average power must remain fixed, we see from Eq. (4.4) that the increase in peak power must be accompanied by a decrease in duty cycle.

In the large ($\gtrsim 1$) SNR case, the sensitivity is improved only by increasing n [i.e., the term 1/SNR in Eq. (4.1) is unimportant]. In this situation,

$$S \approx C_1 \sqrt{n}$$

$$= C_1 \sqrt{\frac{t_m}{t_p}} \tag{4.5}$$

and we see that system sensitivity is improved by making the waveform repetition interval t_p as small as possible.

4.2 Clutter

An obstacle to radar studies aboard the Space Shuttle is unwanted backscatter called ground clutter. This effect can occur not only along the main beam at a range from the satellite to the ground but also through the sidelobes at other ranges to the ground. At high geomagnetic latitudes, auroral and polar cap clutter must also be considered. Both sources are many orders of magnitude stronger than the desired incoherent-scatter signal.

4.2.1 Mainlobe Ground Clutter

Ground-clutter effects can be evaluated by considering the radar cross section, σ, in Eq. (2,1) to have the form[7]

$$\sigma = \sigma^{o} A_{c} \tag{4.6}$$

where

σ^{o} = Radar cross section per unit area intercepted by the antenna beam

A_{c} = Illuminated clutter area.

In Eq. (4.6), σ^{o} is more or less independent of the clutter patch illuminated. A convenient form for σ^{o} that is often used is given by

$$\sigma^{o} = \gamma \sin \varphi \tag{4.7}$$

where

γ = A measure of the clutter cross section

φ = Incidence angle between the radar beam and the local horizontal plane.

The cross-section parameter, γ, is dependent on the ground (or sea) surface conditions. For example, γ is approximately independent of φ for rough terrain, except at near-grazing or near-perpendicular incidence. Typical γ values are between 0.1 and unity.

To estimate the illuminated clutter area, A_c, we consider two cases: (1) short pulsewidth or small φ, and (2) long pulsewidth or large φ. The geometries for the two cases are illustrated in Figure 4.1. The dimension of the illuminated area transverse to the vertical plane shown in Figure 4.1 is $R_c\theta_B$, the same in both cases. The two cases represent approximations where $c\tau/2 \cos \varphi$ is either less than (Case 1) or greater than (Case 2) $R_c\theta_B/\sin \tau$. The illuminated areas for the two cases are then

<u>Case 1</u>:
$$A_c = \frac{R_c\theta_B c\tau}{2 \cos \varphi} \tag{4.8}$$

<u>Case 2</u>:
$$A_c = \frac{R_c^2\theta_B^2}{\sin \varphi} \quad . \tag{4.9}$$

For the two pulsewidths of interest (Section 3)--i.e., 20 and 200 μs--Case 1 (grazing incidence) applies when $\varphi \leq 30°$ and $\varphi < 10°$, respectively. Case 2 applies in situations when φ is greater than the above values.

4.2.1.1 <u>Case 1: Grazing Incidence</u> (Short Pulsewidth)

To obtain an estimate of the clutter power, P_c, we substitute Eqs. (4.7) and (4.8) into the radar equation [Eq. (2.1)]:

$$P_c \approx \frac{P_t \gamma c\tau A \tan \varphi}{8\pi R_c^3 \theta_B} \tag{4.10}$$

where we have let $G_t \approx 4\pi/\theta_B^2$. To obtain the ratio of the clutter power to the power received due to incoherent scatter, P_r, we divide Eq. (4.10) by Eq. (2.10):

$$\frac{P_c}{P_r} = \frac{2\gamma \tan \varphi}{R_c\theta_B N \sigma_o}\left(\frac{R}{R_c}\right)^2 \tag{4.11}$$

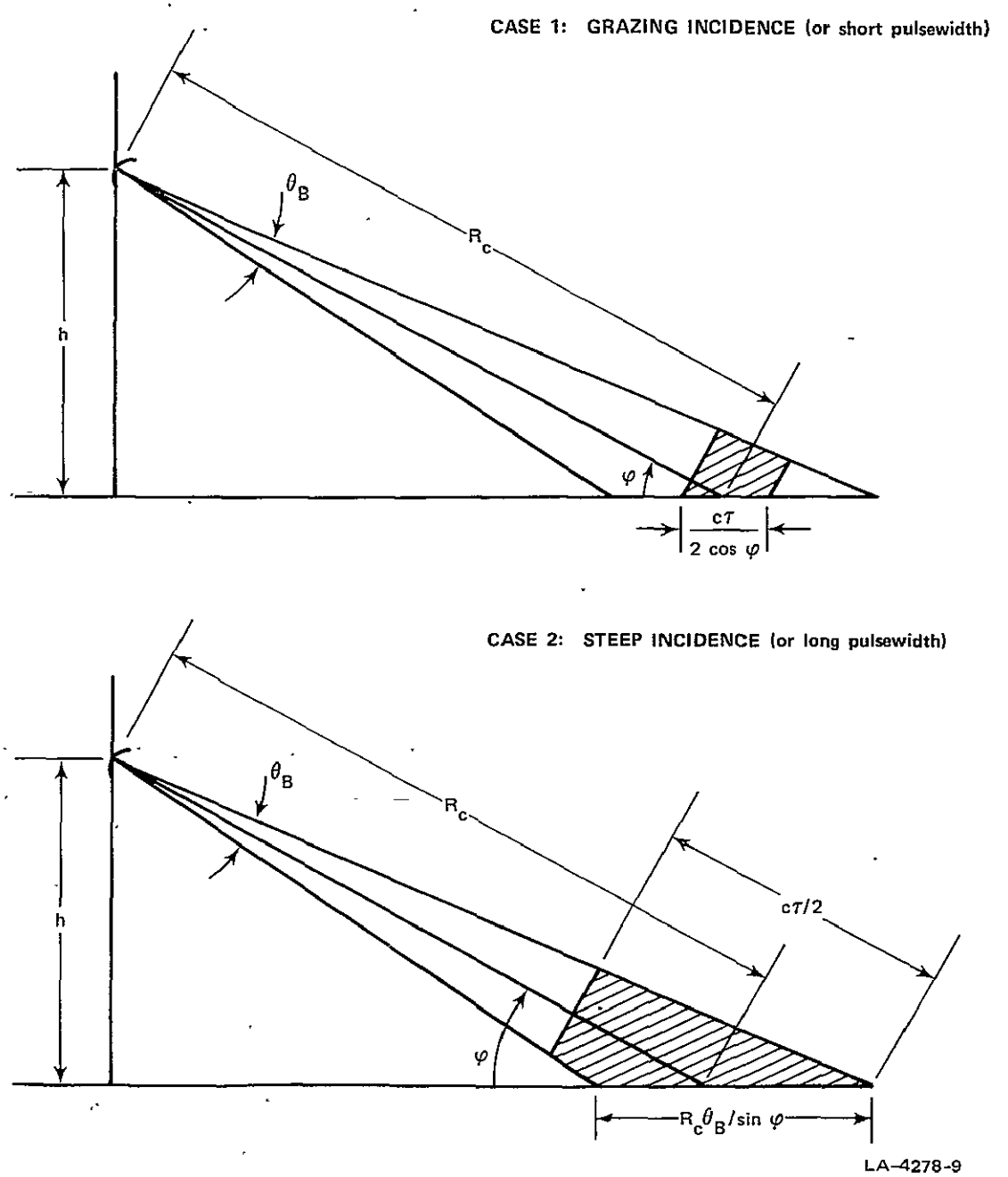

FIGURE 4.1 GROUND-CLUTTER GEOMETRY

ORIGINAL PAGE IS
OF POOR QUALITY

Using the same parameters used in Sections 2.3.2 and 3.0 (i.e., 183-m-diameter antenna, and $N = 10^{11}$ el/m^3), we have

$$\frac{P_c}{P_r} \approx \frac{2 \times 10^{20} \gamma \tan \varphi}{R_c} \left(\frac{R}{R_c}\right)^2 \tag{4.12}$$

For example, if we assume $R_c \approx 10^3$ km, the incidence angle φ for a satellite at an altitude of 300 km is 17°. Then Eq. (4.12) becomes

$$\frac{P_c}{P_r} \approx 7 \times 10^{13} \gamma \left(\frac{R}{R_c}\right)^2 \tag{4.13}$$

Since the incoherent backscatter occurs around $R \approx 100$ to 300 km, we can expect $(R/R_c)^2$ to be between 0.1 and 0.01. From Eq. (4.13), it is clear that the clutter power predominates unless the cross-section parameter, γ, is of the order of 10^{-11} or smaller!

4.2.1.2 Case 2: Steep Incidence (Long Pulsewidth)

A relation similar to Eq. (4.13) can be obtained by substituting Eqs. (4.7) and (4.9) into Eq. (2.1). For the same radar parameters used above, we obtain

$$\frac{P_c}{P_r} \approx 2 \times 10^{14} \gamma \left(\frac{R}{R_c}\right)^2 \tag{4.14}$$

If we increase the pulsewidth to 200 μs, we decrease the above ratio by a factor of 10. That is, the ratio is inversely proportional to the pulsewidth. The power ratio in the steep-incidence (or long-pulsewidth) case is therefore approximately a factor of 2 greater than the grazing-incidence (or short-pulsewidth) case.

4.2.2 Sidelobe Ground Clutter

If we assume that ground clutter enters only from one or a small number ($\lesssim 3$) of sidelobes, the clutter power will be greatly reduced. The reduction factor will be the ratio of sidelobe to mainlobe gain squared times the ratio of the area illuminated by the sidelobes to the area illuminated by the mainlobe, at a given range.

To obtain a rough estimate of the reduction factor, we assume the sidelobe gain to be unity (i.e., isotropic radiation pattern). For the proposed 183-m antenna, the gain-squared ratio is 5×10^{12}. However, the clutter power will be increased by the area illuminated by the isotropic radiator. Using the short-pulse expression (Case 1), since the clutter beamwidth is very large, we have, for the illuminated area,

$$A_{cs} = \frac{c\tau}{2 \cos \varphi} \; 2\pi \, (R_{cs} \cos \varphi) = c\tau\pi R_{cs} \quad . \tag{4.15}$$

The ratio of the illuminated areas for the case of grazing incidence is given by the ratio of Eq. (4.15) to Eq. (4.8):

$$\text{Ratio} = \frac{2\pi \cos \varphi}{\theta_B} \approx 2.3 \times 10^3 \quad . \tag{4.16}$$

The ratio for the case of steep incidence is given by the ratio of Eq. (4.15) to Eq. (4.9):

$$\text{Ratio} = \frac{\pi c \tau \sin \varphi}{R_c \, \theta_B^2} = \frac{\pi c \, \tau h}{(R_c \theta_B)^2} \approx 8 \times 10^3 \quad . \tag{4.17}$$

Therefore, the reduction factor ranges from 10^{-8} in the grazing-incidence case to 4×10^{-8} in the steep-incidence case. The ratio of clutter power in the sidelobes to signal power in the mainlobe then ranges from

$$\frac{P_{cs}}{P_r} \approx 7 \times 10^5 \; \gamma \left(\frac{R}{R_{cs}}\right)^2 \tag{4.18}$$

in the grazing-incidence case to

$$\frac{P_{cs}}{P_r} \approx 8 \times 10^6 \, \gamma \left(\frac{R}{R_{cs}} \right)^2 \tag{4.19}$$

in the steep-incidence case.

From these crude but reasonable estimates, it appears that ground clutter will be a serious problem in the incoherent-scatter radar measurements aboard the Space Shuttle.

4.2.3 Auroral Clutter

In addition to ground clutter, semicoherent backscatter from the auroral E layer represents another source of clutter--i.e., auroral clutter. There is now evidence that auroral clutter will not be limited only to the E layer or the auroral zone, but may very well occur in the auroral F layer and over the polar cap region as well (see Section 5). Auroral clutter has usually not been observed in the auroral F layer or the polar cap E region by ground-based VHF-UHF radars, due to the property of magnetic aspect sensitivity. As the magnetic field lines get more and more nearly vertical, radar beams cannot intersect the magnetic field lines at near right angles. However, from the Space Shuttle it is possible to achieve perpendicularity in the auroral E and F layers and in the polar cap region.

Representative magnetic aspect contours for E-region (h = 110 km) backscatter from a satellite-borne radar at an altitude of 400 km are shown in Figure 4.2. When the satellite is at 50° geographic latitude, a satellite-borne radar obtains auroral E-region clutter from the vicinity of the lower oval band. The boundaries of the oval band correspond to the ±4° magnetic aspect contours. The center contour corresponds to zero magnetic aspect angle.

ORIGINAL PAGE IS
OF POOR QUALITY

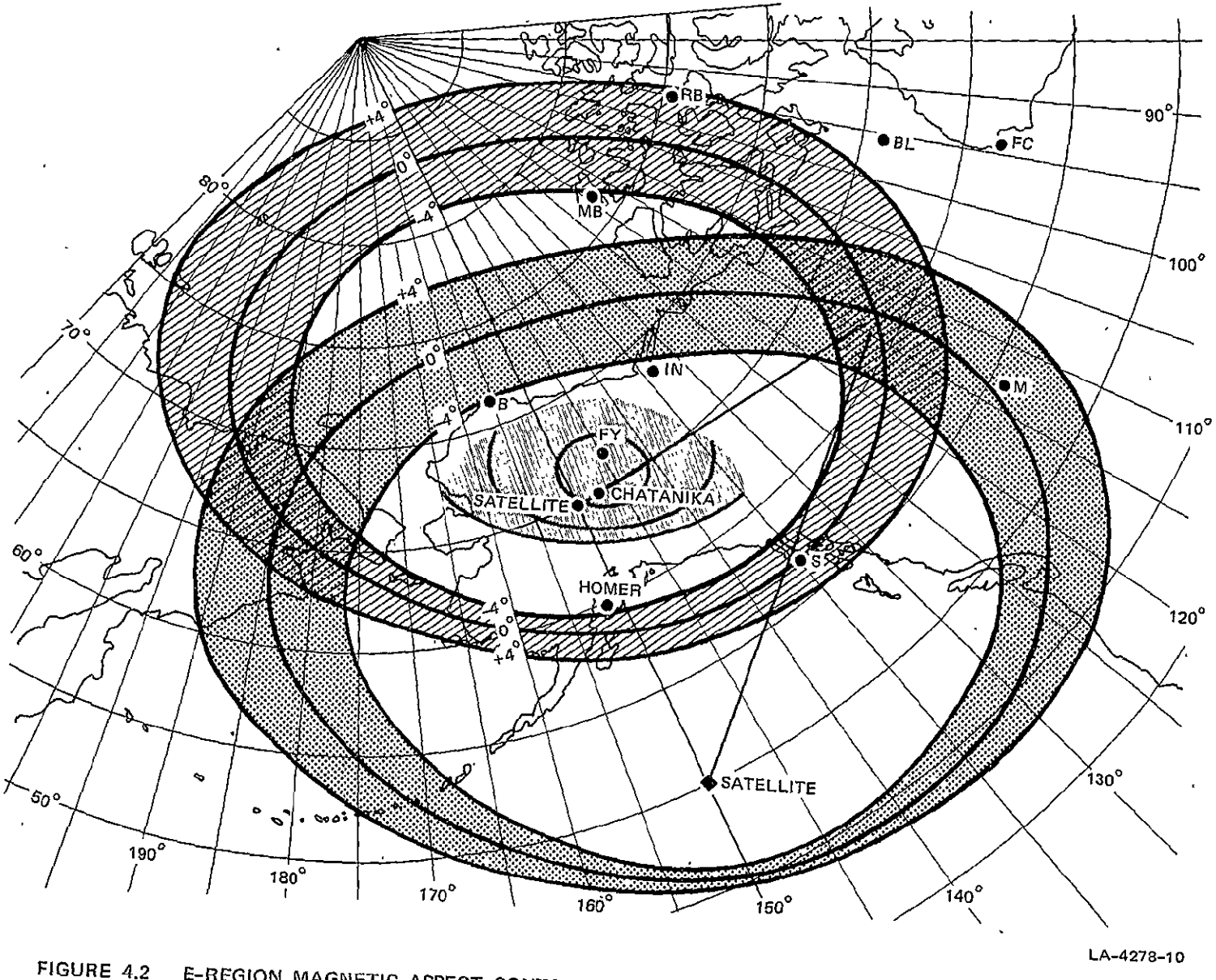

LA-4278-10

FIGURE 4.2 E-REGION MAGNETIC-ASPECT CONTOURS FROM A SATELLITE-BORNE RADAR (h = 400 km)

The average volume scattering coefficient of auroral clutter[8] measured at 448 MHz for a 6-μs chirped pulse was between 10^{-13} and 3×10^{-12} m^2/m^3. In comparison, the volume scattering coefficient for a 400-μs pulse was 10 dB less. If we compare these values to an incoherent-scatter coefficient of 3×10^{-18} m^2/m^3, assuming an electron density of 10^{11} el/m^3, we find that the average auroral clutter exceeds the desired signal by 60 dB and probably by 70 dB or more during more intense auroral activity. Therefore, auroral clutter is easily comparable in strength to ground clutter that enters through the sidelobes.

On the other hand, due to the magnetic aspect dependence of auroral E-region clutter, its contribution is drastically reduced as the radar beam is directed away from exact perpendicularity to the magnetic field lines. Chesnut et al.[9] found a 10-dB/deg magnetic aspect dependence around the zero magnetic aspect angle that was more or less independent of wavelength. For off-perpendicular angles between 4.5° and 7.5°, Jaye et al.[8] found 4 to 6 dB/deg magnetic aspect dependence.

The above estimates are for the case of auroral E-region clutter that enters through the mainlobe at the same range as the incoherent-scatter signal. Furthermore, we have assumed that auroral clutter is obtained from a scattering volume of the same size as that of the incoherent-scatter. To check this assumption, we selected the maximum slant range shown in Figure 4.2, which is approximately 2500 km. For a 183-m-diameter antenna, or a beamwidth of 0.16°, the transverse dimension is approximately 7 km, of the order of the thickness of the scattering layer. Therefore, the assumption that the volume is filled is valid.

In addition to auroral and polar cap E-region clutter, we may expect to encounter auroral (and possibly polar cap) F-region clutter. Although this type of clutter has not been observed experimentally due to the magnetic aspect limitations of ground-based radars, it may very

well represent a more serious source of clutter since its location may correspond in range with the desired incoherent-scatter signal.

4.2.4 Clutter Mitigation

It is obvious that clutter will be a severe problem if it arrives at the receiver at the same time as the signal. It is also apparent that conventional clutter-cancelling techniques will not be sufficiently effective in removing clutter 50 or more dB stronger than the incoherent-scatter signal, and potentially spread in frequency.

The most straightforward approach is to vary the waveform repetition period such that the data of interest do not appear at the same time as the clutter. (Since E-region auroral clutter occurs only in restricted regions and will often be at slant ranges comparable to that of the ground clutter, we consider only the ground clutter.) If each succeeding transmitted waveform is to follow the final arrival of ground clutter, we must compute the maximum slant range of the ground clutter. The maximum range to the ground clutter, R_{max}, is taken to be the distance from the spacecraft to the point on the ground where the radar beam is tangent to the earth's surface. That range is given by

$$R_{max} = \left[(r_e + h)^2 - r_e^2\right]^{1/2} \tag{4.20}$$

where r_e is earth's radius, and h is the altitude of the spacecraft. R_{max} is plotted as a function of h in Figure 4.3. Also shown are the waveform repetition period and the waveform repetition rate. For typical satellite altitudes, the waveform repetition period must be greater than 15 ms. In this case, the received signal within waveform repetition interval will look like that shown in Figure 4.4.

An alternative clutter-mitigation technique is to shift the transmitter/receiver frequency such that the backscatter associated with

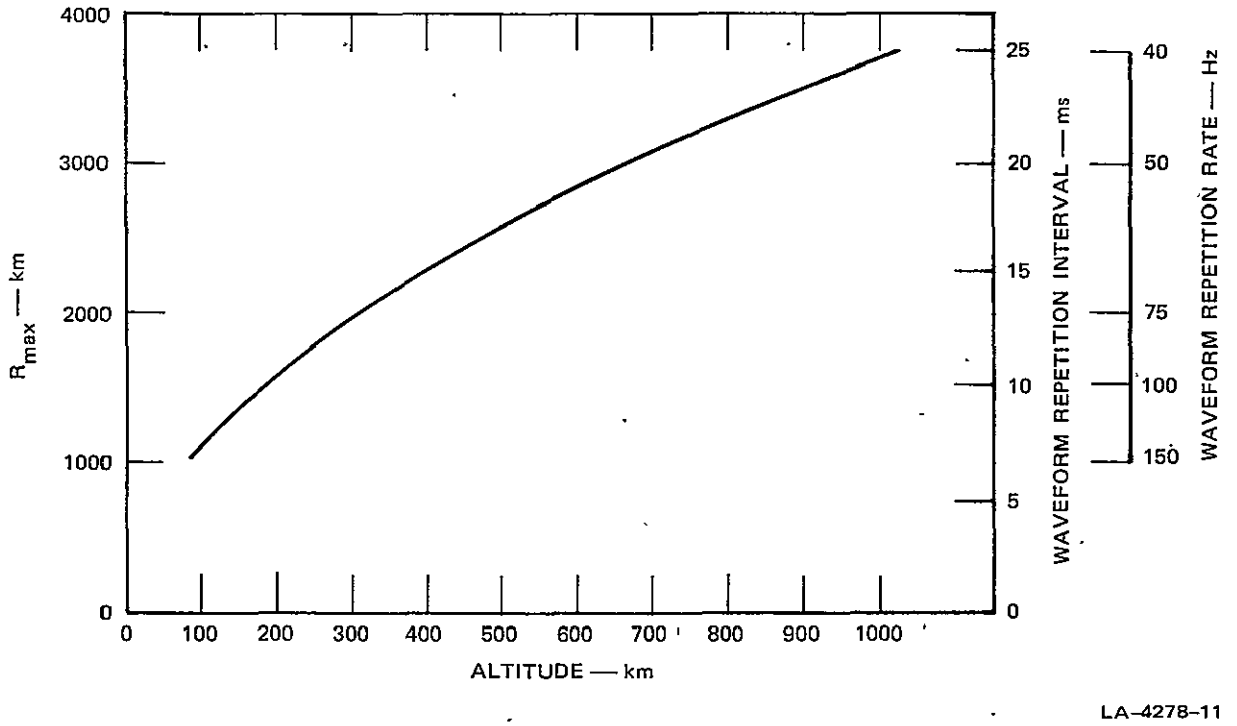

FIGURE 4.3 MAXIMUM GROUND-CLUTTER RANGE DEPENDENCE ON SPACECRAFT ALTITUDE

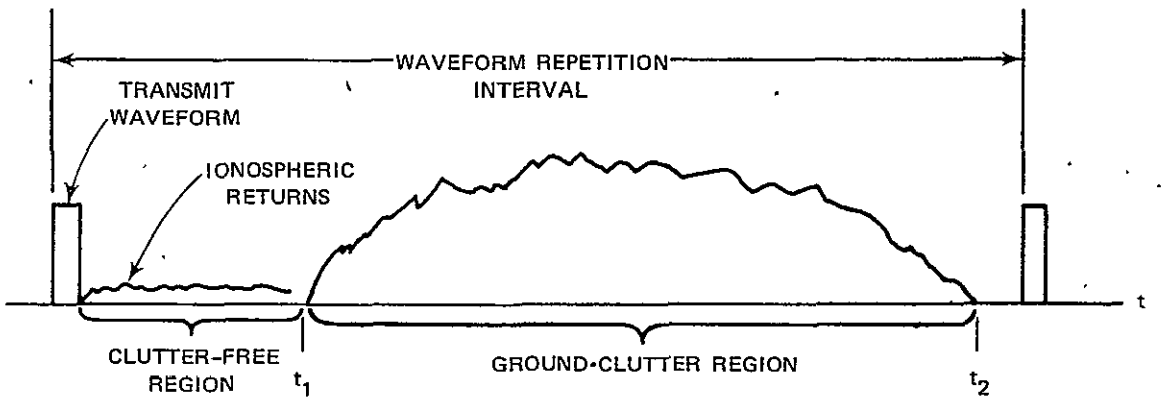

WHERE t_1 = TIME DELAY (~300 km)

t_2 = TIME DELAY (~15 ms) CORRESPONDING TO R_{max}

LA-4278-12

FIGURE 4.4 REPRESENTATIVE IONOSPHERIC AND GROUND-CLUTTER RADAR SIGNAL RETURNS

a previous transmission falls outside the frequency band associated with the succeeding transmission. In this way, the waveform repetition period can be arbitrarily shortened by sequential transmission of the appropriate number of different frequencies. In order to evaluate the feasibility of this technique, we need to know the magnitude of the required frequency displacement. If we assume a square pulse of length τ, it will have a frequency power spectrum given by

$$S_\tau(f - f_o) = \left[S_o \frac{\sin \pi(f - f_o)\tau}{\pi(f - f_o)\tau} \right]^2 \tag{4.21}$$

or

$$S_\tau(\Delta f) = S_o^2 \left(\frac{\sin \pi \Delta f \tau}{\pi \Delta f \tau} \right)^2 \quad . \tag{4.22}$$

The contribution of the power spectrum transmitted with a center frequency, f_o, at a displaced frequency, f, is determined by the envelope of the sinusoid. That is, $S_\tau(0)/S_\tau(\Delta f)$ is proportional to $(\pi \Delta f \tau)^{-2}$. This relationship is plotted for τ's of 20 and 200 μs in Figure 4.5. It is evident from the figure that in order to reduce the clutter power by six orders of magnitude, the frequency must be shifted by 2 to 20 MHz. To utilize such a technique, both transmitter and receiver must be capable of being rapidly tuned. Furthermore, the antenna must be capable of efficient operation over the frequency range of interest.

4.3 Averaging Time vs Spatial Resolution

In the evaluation and selection of radar design options for an incoherent-scatter radar aboard the Space Shuttle, we must consider the required averaging times and their consequences in terms of spatial resolution. As discussed in Section 4.1, it is desirable to have two modes of transmitter operation: (1) high peak power, and (2) high duty cycle. The first mode of operation is desirable when the SNR is much less than unity.

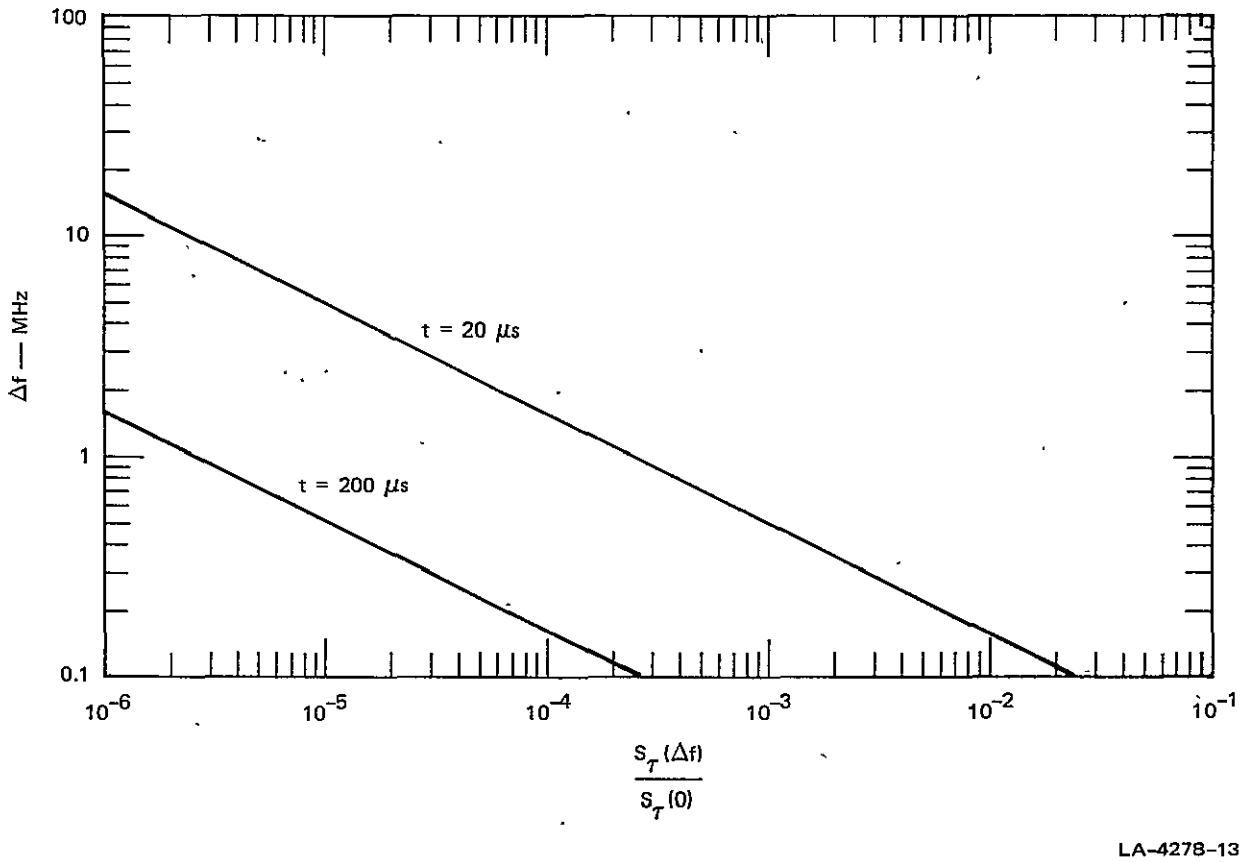

FIGURE 4.5 FREQUENCY POWER SPECTRUM AS A FUNCTION OF f, τ

System sensitivity is most efficiently improved in that case by increasing the peak power. Once the SNR is of the order of unity, the second mode of operation is most efficient in further increasing the system sensitivity. However, as discussed in Section 4.1, high peak powers can be achieved only at the expense of a lowered duty cycle. Because a radar on board the Space Shuttle is moving at orbit velocities, a low duty cycle results in reduced spatial resolution.

The satellite-borne radar will be moving at a velocity of about 8 km/s relative to the ionosphere. If the radar beam is pointed perpendicular to the spacecraft velocity vector, each individual transmitted pulse will probe a displaced region of space. Consider the 183-m antenna, which produces a beamwidth of about 0.16°. At a range of 100 km, this corresponds to a 300-m-diameter cross-sectional area. This means that in

37.5 ms, a completely new volume of space is probed. Thus, when averaging times in excess of 37.5 ms are used, as they most probably will be, the spatial resolution of the radar measurement will be spread out in the direction of the spacecraft velocity. The spatial resolution cell will be determined by:

(1) The pulse length in the direction along the radar beam.

(2) The beamwidth in the direction mutually perpendicular to the beam and the velocity vector.

(3) The product of the spacecraft velocity times the averaging (integration) time in the direction of the velocity vector.

Clearly, the averaging time, and hence the spatial resolution, is directly dependent on the waveform repetition rate. Since the Space Shuttle is average-power-limited, we cannot expect to arbitrarily increase the waveform repetition rate to suit all needs. We will show in the following section, based on power-aperture-product requirements, that the waveform repetition period cannot be less than 2.67 ms and will be proportionately longer with any increase in peak power requirements. An even longer repetition period is required if clutter is to be kept outside of the range interval containing the incoherent-scatter signal (see Section 4.2.4). If no other clutter-mitigation technique is used, the minimum waveform repetition period will be 15 ms (or a PRF of 67 s^{-1}). Therefore, with the waveform repetition period restricted to values between 2.67 and 15 ms (and possibly even longer due to higher-peak-power requirements), we can expect to obtain only 2.5 to 14 samples in the time it takes the spacecraft to move one beamwidth.

Perhaps a more reasonable criterion would be to average over a time such that the resolution in the velocity-vector direction equaled the resolution along the radar beam. For a 20-μs pulse (3 km), the averaging time would still be 37.5 ms; for a 200-μs pulse (30 km), the averaging time

would be 375 ms. Therefore, in the long-pulse mode, we can expect a tenfold increase in the number of samples, or 25 to 140 samples.

Similar considerations come into play when the radar beam is pointed parallel (or antiparallel) to the spacecraft velocity vector. In this case, one could consider compensating in the data processing for the constantly changing range of a particular segment of the ionosphere. Although possible, this procedure may not be particularly beneficial because those few samples taken at the closest range (and thus highest SNR) will contribute most heavily to the averages.

Let us assume that peak power can be increased arbitrarily such that SNRs of the order of unity can be achieved. We can then compute the spatial resolution that will ultimately be limited by the number of required samples. A reasonable number would be 400 samples when SNR=1. If a clutter-cancelling technique could be employed, 400 samples taken with a a 2.67-ms waveform repetition period would give a minimum spatial resolution along the velocity vector of 8.5 km. If clutter remains a problem, the minimum spatial resolution based on a 15-ms waveform repetition period would be 48 km.

4.4 Transmitter

When evaluating the transmitter requirements for a satellite-borne incoherent-scatter radar, we must consider the average available power, the required peak powers, the modes of transmitter operation, and the optimum operating frequencies. As noted in Section 4.1, the Space Shuttle radar will be average-power-limited. In order to optimize its utilization, we discussed radar modes of operation in Section 4.1 based on the SNR and the minimization of the standard deviation associated with the mean incoherent-scatter return. For low SNRs, it is desirable to operate the transmitter in a high-peak-power (and if necessary, a low-duty-cycle)

mode. For high SNRs, just the converse is true. Also based on SNR considerations, we found in Section 2.3 that the operating frequency of an incoherent-scatter radar on the Space Shuttle would best be placed in the 300-to-1000-MHz range.

Let us consider the high peak power since it impacts directly on transmitter design. As discussed in Section 2.3.2, reasonable SNRs can be achieved with a power-aperture product, P_tA, between 10^8 and 10^9. For a P_tA of 10^8 and the assumed maximum aperture based on the availability of a 183-m-diameter antenna, the peak power required was found to be approximately 10 kW. The Spacelab Payload Accommodation Handbook[10] states that about 4 kW of average power is available to experiments. Let us assume that 2 kW of the 4 kW of average power available to Space Shuttle experiments can be used for the incoherent-scatter radar transmitter. To arrive at average transmitter power available, we have also to consider power-converter and transmitter efficiencies. The former can be expected to be no better than 75%, and the latter no better than 50%. Thus, at best the transmitter average power output would be 750 W. If the peak power is to reach 10 kW, the duty cycle could be no greater than 7.5%. For higher peak powers, the duty cycle must be proportionately reduced. For 100 kW peak power, the duty cycle could be no greater than 0.75%. Even higher peak powers may be required in the event that the size of the usable antenna is limited to less than the assumed 183-m antenna.

If only 10 kW of peak power is required, the waveform repetition period for a 200-μs pulse can be as short as 2.67 ms if the presence of clutter can be mitigated. However, if the clutter-mitigation techniques are ineffective, the presence of clutter forces us to use a minimum waveform repetition interval of 15 ms. The corresponding peak power allowed in this case is 56 kW.

To place a reasonable limit on a desirable transmitter peak power, we have to evaluate the SNR equation for the shortest pulse to be transmitted. As discussed in Section 3.1, we will take 20 μs for the shortest pulsewidth. Still assuming the use of a 183-m antenna, and for a range of 300 km, an SNR of 0.5 when looking away from the earth and 0.15 when looking toward the earth can be achieved with a peak power of 1 MW at 600 MHz. For a range of 100 km, a peak power of 100 kW would achieve the same SNRs. The SNRs are only slightly different for frequencies between 300 and 1000 MHz.

The above discussion bounds our transmitter selection to an average power of less than 1 kW, a peak power of at least 10 kW (but preferably 100 kW, or even 1 MW), a pulse length of less than 1 ms, and a frequency range of 300 to 1000 MHz. In general, klystrons, traveling-wave tubes, grid-controlled tubes, and some crossed-field devices could meet the bounded transmitter requirements outlined above. For 10-kW peak powers, typical tube weights are around 50 lb and beam voltages around 10 kV. For 100-kW peak powers, these numbers go up to 200 lb and 30 kV. For 1-MW peak powers, the numbers are up to 800 lb and 100 kV.

The beam voltage requirement also impinges on the conversion to that value from the spacecraft's prime power of 28 Vdc. Converters from 28 V to 1 kV for power levels up to 1 kW are commercially available, and converters to tens of kilovolts are certainly within the state of the art. Converter weight would be of the order of 10 lb/kW. Using this number as a rule of thumb, converter weight will be 1000 lb at 100 kW peak power and 10,000 lb at 1 MW peak power. Modulator weights will vary strongly, depending on duty cycle and waveform repetition-rate requirements.

While peak power of the order of a megawatt is readily achievable with conventional transmitters, the duty cycle becomes unacceptably low if we would like to maintain a spatial resolution of 50 km (along the

velocity vector), or less. Another problem that arises when the peak powers approach the megawatt-to-tens-of-megawatts range is antenna breakdown due to the high RF electric fields. This problem is considered in Section 4.6. The possible sequential requirement of high variation of peak powers from the same transmitter also presents problems; at best a 10-dB variation in peak power can be achieved without drastic loss in transmitter efficiency. To arrive at a particular design that can meet most of the requirements of the incoherent-scatter radar aboard the Space Shuttle, we need to make a detailed study of several specific transmitter designs.

4.5 Energy-Storage Considerations

A means of overcoming the average power limitation (and hence, increasing the duty cycle while maintaining a given peak power) is to utilize an energy-storage device, an example of which might be a large capacitor bank. To estimate the amount of energy that would have to be stored, we assume that 400 samples are required. Then for a 200-μs pulsewidth and 1 MW peak power, we will require 8×10^4 joules. To cover various uncertainties such as the possible use of higher peak powers, smaller antennas, and so forth, a reasonable amount of stored energy would be 10^5 to 10^6 joules.

Let us consider how a megajoule of energy could be utilized. As above, we assume that 400 samples are required. Then, given the pulsewidth, we can determine the maximum peak power that can be used so that all of the energy will be expended after the 400th pulse. For a 200-μs pulse, the corresponding peak power is 12.5 MW. The peak power corresponding to a 6-pulse-burst waveform, with each pulse being of 20-μs duration, is 20.8 MW. Since we are only interested in increasing the peak power to a value such that the SNR is of the order of unity, we may consider to what extent the antenna size may be reduced, given the above peak powers. For

an SNR of unity at 100 km range for an electron density of 10^{11} el/m^3, the mean of the power-aperture product for the space-oriented sector and that for the earth-oriented sector is 1.3×10^8. Using this number, we find that only a 17-ft (5.2-m) diameter antenna is required. Similar computations for the burst waveform reveal that a 73-ft (22.2-m) diameter antenna is required.

The use of an energy-storage device implies that a recharging time must be associated with it. For example, using 1 kW average power, it would take approximately 1000 s to recharge the megajoule energy bank. If we assume a 100-minute orbital period for the Space Shuttle, we would be able to conduct six experiments per orbit. Clearly, it would not be advantageous to expend the total available energy to achieve maximum peak powers and minimum-sized antennas. Instead, the required power-aperture product should be achieved with reasonable peak powers and maximum antenna apertures that are cost-effective. For example, of the megajoule of available energy, 100 kJ might be expended for each experiment, thus increasing the number of experiments per orbit to approximately 60 instead of 6. With that amount of energy, a peak power of 1.25 MW and a 54-ft (16.5-m) diameter antenna could be used to attain the desired power-aperture product for a 200-μs pulse. For the burst waveform, the corresponding peak power would be 2 MW and the antenna diameter would be 230 ft (70.1 m). The above results are summarized in Table 4.1.

An important question that must be answered is what would be the weight and size of a megajoule energy bank? For order-of-magnitude estimates, let us consider the use of a capacitor bank. If we assume the operating voltage to be 10 kV, we will require a capacitance of 2×10^{-2} F. If we further assume that a microfarad capacitor with 10-kV voltage rating weighs approximately a pound, the total weight must be of the order of 20,000 lb. The size is estimated to be of the order of 35 m^3 (i.e., 3.3 m to a side). These numbers are based on estimates of commercially available

Table 4.1

POWER-APERTURE REQUIREMENTS, GIVEN ENERGY-STORAGE CAPABILITIES AND RADAR WAVEFORMS

Waveform	Case 1 Energy Available = 10^6 Joules		Case 2 Energy Available = 10^5 Joules		Resolution Achieved (km)		
	Peak Power	Antenna Diameter	Peak Power	Antenna Diameter	$c\tau/2$	νt	$R\theta_B$
200 μs	12.5 MW	17 ft	1.25 MW	54 ft	30	45	$\begin{pmatrix}10\\3\end{pmatrix}^*$
20-μs burst	20 MW	73 ft	2 MW	230 ft	3	45	$\begin{pmatrix}2\\0.7\end{pmatrix}^*$
Recharge time	$\sim 10^3$ s		$\sim 10^2$ s				

SNR = 1.0 at 100 km for 10^{11} el/m^3.

*The upper number in parentheses corresponds to the antenna diameter for Case 1, and the lower number corresponds to the antenna diameter for Case 2.

capacitors and therefore are intended only to help conceptualize the idea of an energy storage device. The weight amounts to two-thirds of the total payload capacity of the Space Shuttle Orbiter.[10] A detailed study would be required to evaluate the feasibility of the capacitor bank as a means of alleviating the average-power limitations on board the Space Shuttle.

4.6 Antenna

4.6.1 Antenna Size and Weight

Of the various tradeoffs available to optimize the SNR for the incoherent-scatter experiment on the Space Shuttle, the most appealing is the use of large antenna apertures. The average-power limitation on the Space Shuttle makes this an important consideration. With a large aperture, transmitters with reasonable peak powers can be used. Furthermore,

shorter waveform repetition periods can be used to minimize the averaging time and improve the spatial resolution. However, in considering large antenna apertures, we must keep in mind the space and weight limitations on the Space Shuttle.

In a study conducted by the Lockheed Missiles and Space Company,[5] a wrap-rib parabolic antenna that unfurls to a 600-ft (183-m) diameter and is capable of being mechanically steered is expected to be available by 1985. When furled, this package fits into a 15-ft-diameter by 2-foot-long envelope. The antenna weight at an operating frequency of 2 GHz with the maximum size rib studied is 10,000 lb. In comparison, the Space Shuttle Orbiter can accommodate within its bay a payload 15 ft in diameter by 60 ft long weighing approximately 32,000 lb. This total payload weight is based on a circular polar orbit at an altitude of approximately 400 km. Therefore, the antenna weight would represent about one-third the total payload weight.

4.6.2 Antenna Deployment and Steering Considerations

In order to clear the rudder of the Space Shuttle Orbiter, a short (approximately 45-ft) tower is required, which can be tilted up after the payload doors are opened. The furled antenna would be secured to the end of this tower. Such an antenna structure is illustrated in Figure 4.6. With the antenna rigidly mounted on the tower, the antenna would be steered by varying the attitude of the Orbiter itself. For this purpose, it is envisioned that the three-axis vernier Reaction-Control-System (RCS) jets would be used.[11] For this kind of configuration and control, the maximum slewing rate of the antenna would be 0.1°/s with a ±0.5° pointing accuracy. The acceleration rates must be less than 10^{-3} rad/s^2 with the RF off, and less than 7×10^{-5} rad/s^2 with the RF on.[5] This means that 25 s will be required to attain the 0.1°/s slewing rate, and that it will take about 15 minutes to rotate the antenna through an angle of 90°.

ORIGINAL PAGE IS
OF POOR QUALITY

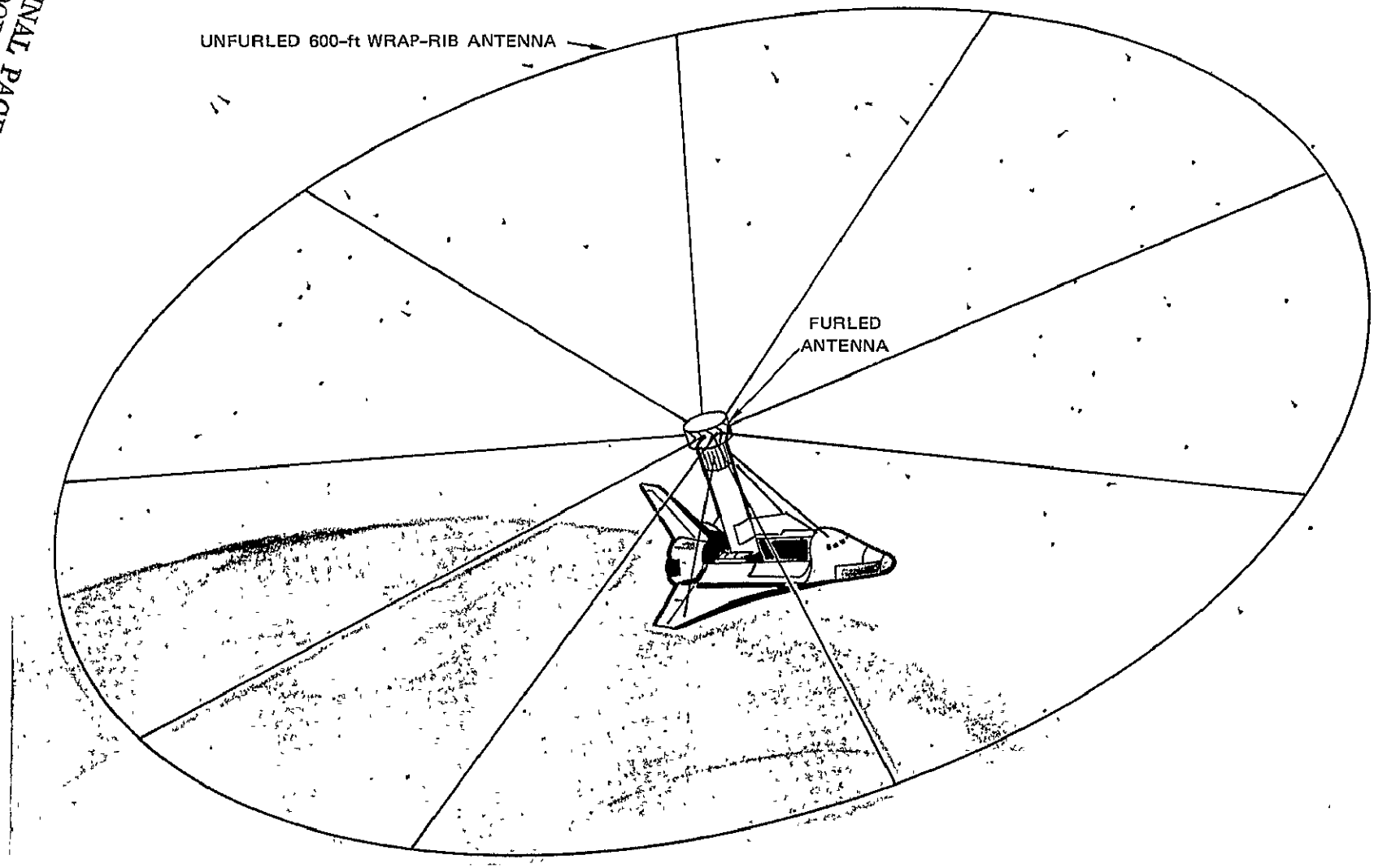

LA-4278-14

FIGURE 4.6 ARTIST'S DRAWING OF 600-ft UNFURLED ANTENNA AND SPACE SHUTTLE

A possible alternative is to use a 100-m telescoping tower with the furled antenna in a double-gimbal arrangement (i.e., X-Y mount) at one end of this tower.[12] Then through the use of electric motors to rotate the antenna, a slewing rate of 0.5°/s could be attained. However, the same maximum acceleration rates mentioned above must not be exceeded.

4.6.3 Atmospheric Drag on Large-Aperture Antennas

When structures with large cross-sectional area are deployed from a satellite, the effects of atmospheric drag on the satellite's orbit must be considered. In particular, we will be concerned with the loss of altitude with time due to air drag on the above-described, unfurlable parabolic reflector. The air-drag force, F_D, is given by[13]

$$F_D = \frac{1}{2} C_D \rho v^2 A \mu \tag{4.23}$$

where

C_D = Drag coefficient (= 1.2)

ρ = Air density

v = Vehicle velocity

A = Projected surface area in direction of the velocity vector

μ = Mesh factor.

The mesh factor is a measure of the effectiveness of the structure in blocking the air flow. For a circular orbit, the vehicle velocity, v, is given by

$$v = r_e \sqrt{\frac{g_e}{r_e + h}} \tag{4.24}$$

where

r_e = Earth's radius (=6371 km)

g_e = Gravitational acceleration on the earth's surface = 9.8×10^{-3} km/s^2

h = Altitude of the vehicle.

At a frequency of 1 GHz, the woven surface of an unfurlable antenna has a mesh factor of 0.2 when the antenna boresight is parallel to the velocity vector.[12] The transmission of the mesh $(1 - \mu)$ decreases as a function of the cosine of the angle, φ, between the antenna boresight and the direction of travel for small angles. When φ is 65°, the transmission is 20%, and when φ is 75°, the transmission is 15%. Finally, at $\varphi = 80°$, the surface is considered closed (i.e., $\mu = 1$).

Figure 4.7 shows a plot of drag force versus antenna diameter with altitude as a parameter computed from Eq. (4.23). In order that we may use the results as an upper bound on the drag force, a high-density atmosphere was used.[14] Since A is a function of the square of the reflector diameter, the curves are straight lines with a slope of 2 when plotted on log-log paper. The drag force may be counteracted by the propulsion system aboard the Space Shuttle.[15] The maximum available impulse with three additional Payload Bay kits[10] is noted on Figure 4.7.

If the drag force is not counteracted, its effect may be calculated using perturbation techniques.[13] The decrease in altitude, ξ, is given by

$$\xi = - \frac{C_D A'}{m} \rho r_o^2 \left(1 - 2 \frac{\Omega}{\dot{\theta}} \cos i_o\right) \theta \qquad (4.25)$$

where

A' = Effective projected surface area $(A \times \mu)$

m = Total mass of Orbiter and antenna
= 250,000 lb[12]

r_o = Radial distance of vehicle from the center of the earth at zero time

Ω = Earth's rotation rate, in rad/s

θ = Central angle of orbit

$\dot{\theta}$ = Orbital rate at r_o

i_o = Inclination of orbital plane to equatorial plane.

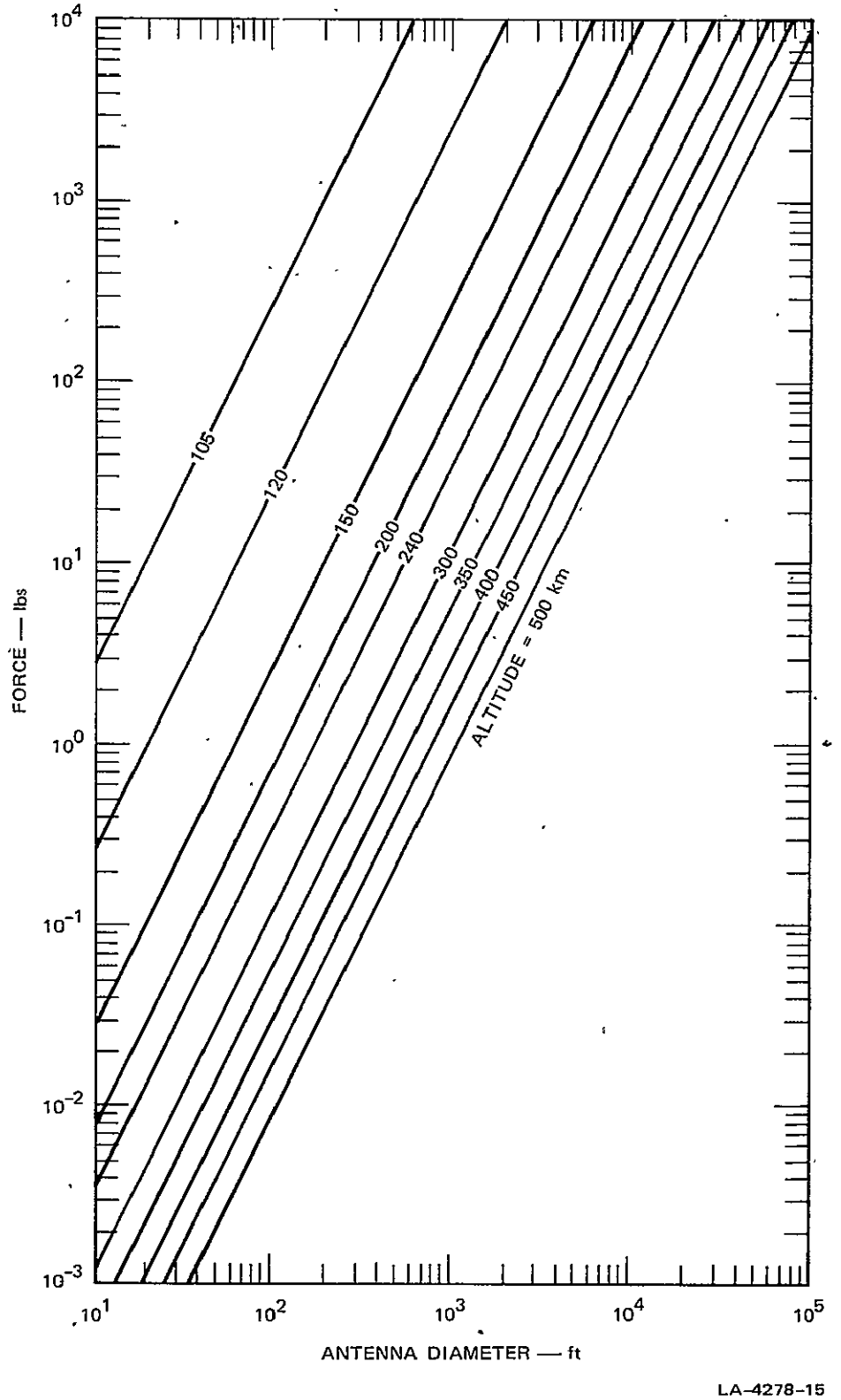

FIGURE 4.7 DRAG FORCE AS A FUNCTION OF ANTENNA DIAMETER AND SPACECRAFT ALTITUDE

For the cases in which ξ is much smaller than the mean altitude of the spacecraft, the value of air density, ρ, may be considered constant. Figure 4.8 shows a plot of ξ versus time with antenna diameter as a parameter. In this plot, we have assumed an initial vehicle altitude of 300 km and a zero-degree orbital inclination, and have neglected the small change in orbital inclination with time. Since the air density decreases much faster than r_o^2 or $r_o^2 \dot{\theta}$ as the initial altitude is increased, ξ is smaller at higher initial altitudes. We also see from Eq. (4.25) that ξ is a maximum when the satellite is in a polar orbit.

4.7 Antenna Breakdown Considerations

In dealing with high powers, antenna breakdown due to ionization produced by the intense RF electric fields must be considered. Breakdown occurs when the rate of electron production exceeds the rate of electron loss. If a CW field is applied, the electron density tends to grow indefinitely until the partially ionized gas begins to act as a reactive and absorptive medium for RF fields, thus modifying the fields that cause the ionization. This occurs in the vicinity of the critical electron density, $N_c \approx 10^{10} f^2$, where N_c is in el/m^3, and f is the frequency in megahertz. Breakdown is usually said to occur when the plasma becomes overcritical, causing a precipitous drop in the power radiated beyond the plasma.[16]

If the high-power field is applied in short pulses, the electron production rate must exceed the electron loss rate sufficiently so that the electron density becomes overcritical before the end of the pulse. This means that the thresholds for pulse breakdown are higher than for the corresponding CW case. Therefore, to evaluate the worst case, we consider only the CW breakdown case.

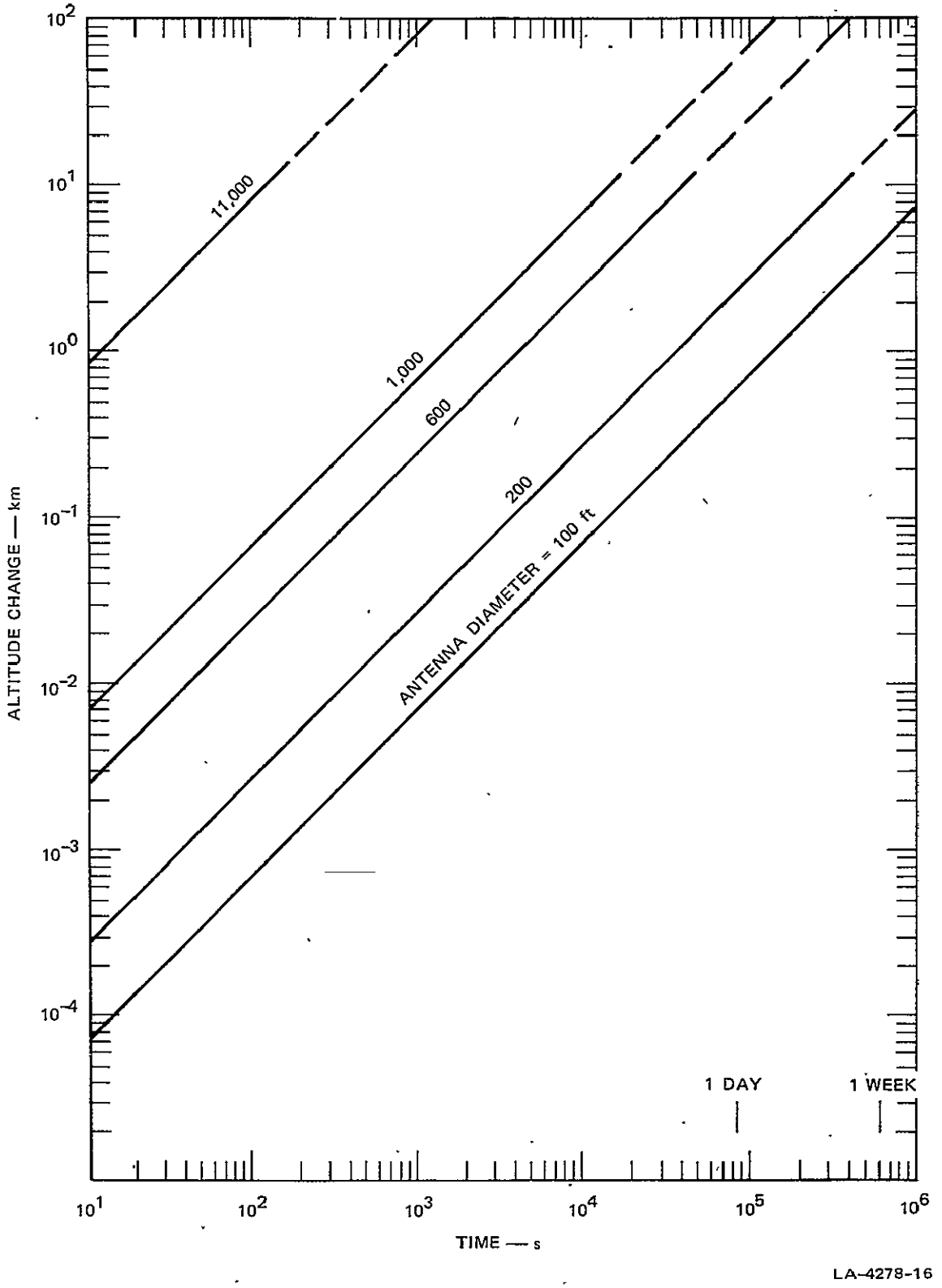

FIGURE 4.8 SPACECRAFT ALTITUDE DECREASE AS A FUNCTION OF TIME AND ANTENNA DIAMETER

4.7.1 Gas Discharge Breakdown

The general breakdown equation is given by the electron-density continuity equation

$$\frac{\partial N}{\partial t} = (\xi - \beta)N + S_i + \nabla^2(DN) - \alpha N^2 \tag{4.26}$$

where

β = Attachment-rate coefficient

ξ = Ionization rate

D = Diffusion coefficient

S_i = External source of ionization rate

α = Recombination-rate coefficient

N = Electron density.

The breakdown threshold can be determined from Eq. (4.26) by setting $\partial N/\partial t = 0$. The electric field strength associated with the breakdown threshold can then be computed from an established empirical relationship between the rms electric field and the ionization rate.[17] That relationship is given by

$$\frac{\xi - \beta}{p} = 4 \times 10^7 \left[\frac{(E_e/p)}{10^2}\right]^{5.33} - 6.4 \times 10^4 \tag{4.27}$$

where

p = Pressure

E = rms electric field strength

$E_e = E(1 + \omega^2/\nu_c^2)^{-1/2}$

ν_c = Electron-neutral collision frequency.

At an altitude of 200 km, recombination is negligible. Furthermore, we neglect the presence of any external source of ionization. Equation (4.26) is then reduced to

$$\xi - \beta = -\frac{1}{N}\nabla^2(DN) \quad . \tag{4.28}$$

When the electron density is low, electrons diffuse freely. However, in the ionosphere where both electron density and ion density are high, ambipolar diffusion dominates. The study of Allis and Rose[18] indicates that when the initial electron density, N_o, is equal to or greater than $10^{-4}N_p$, a correction must be made for ambipolar diffusion. N_p is the electron density for which $\omega = \omega_p$, where ω = angular radar frequency, and $\omega_p^2 = Ne^2/\epsilon_o m$. For a radar frequency of 600 MHz and an electron density (N_o) of 10^{12} el/m^3, we find that $N_p = 4.5 \times 10^{15}$ el/m^3 and $N_o = 2 \times 10^{-4} N_p$. Therefore, the effects of ambipolar diffusion must be considered.

The ambipolar diffusion coefficient, D_a, is given by

$$D_a = 2D_- \frac{\mu_+}{\mu_-} \tag{4.29}$$

where μ_+, μ_- are the mobilities of the ions and electrons, respectively, and D_- is the free electron diffusion coefficient. The ions of interest are N_2^+ and O^+. However, since the effect of ambipolar diffusion is to lower the breakdown level, we consider the worst-case conditions--i.e., only N_2^+ ions. A reasonable extrapolation beyond measured values for the mobilities[19] is $D_a = D_-/90$. The electron diffusion coefficient is given by

$$D_-p = 3.2 \times 10^{-6}\ \bar{u}_e \tag{4.30}$$

where

p = Pressure

$\bar{u}_e$ = Average electron density.

At an altitude of 200 km, assuming a gas mixture of 43% N_2, 47% O, 6% O_2, and 0.07% each of He and A, the reduced pressure based on particle density[20] is 2.33×10^{-7} torr. If 5 eV is used as the typical electron energy, $D_- \approx 6.18 \times 10^{12}$. Therefore, the ambipolar diffusion coefficient is 6.87×10^{10} cm^2/s.

To simplify Eq. (4.28), we assume an exponential variation in electron density with a characteristic diffusion length, Λ, such that $\nabla^2 N = N/\Lambda^2$. Equation (4.28) becomes

$$\xi - \beta = -\frac{D}{\Lambda^2} \quad . \tag{4.31}$$

At very low pressures, where the electron mean free path is much greater than the dipole radius, the breakdown region expands away from the dipole and approximates a sphere about the antenna. Thus, an appropriate diffusion length, Λ, is of the order of $\lambda/2$, the antenna dimension, rather than the usual dipole radius dimension. At 600 MHz ($\lambda = 0.5$ m),

$$\frac{D}{\Lambda^2} = \frac{4D}{\lambda^2} = \frac{6.87 \times 10^{10}}{25^2} = 1.1 \times 10^8 \ s^{-1} \quad . \tag{4.32}$$

For air, $\beta \sim 4 \times 10^{-6} \ \nu_c$, where ν_c is the electron-neutral collision frequency given by $\nu_c = 5.3 \times 10^9 p$. Therefore, the attachment rate, β, is given by $\beta \sim 2.1 \times 10^4 p$ or $\beta \sim 0.005 \ s^{-1}$. Therefore, the ionization rate is approximately $1.1 \times 10^8 \ s^{-1}$.

Extrapolation of cold-air breakdown data gives

$$\begin{aligned} \left(\frac{E_e}{p}\right) &\approx \left(3300 \ \frac{\xi}{p}\right)^{1/5.62} \\ &\approx \left[(4.72 \times 10^{14})(3300)\right]^{1/5.62} \\ &\approx \quad 1726 \end{aligned} \tag{4.33}$$

$$\frac{E_e}{p} = \frac{E_{rms}}{P(1 + \omega^2/\nu_c^2)^{1/2}} \approx 1726 \tag{4.34}$$

or

$$E_{rms} \approx \frac{1726\ \omega p}{\nu_c} \approx 1228\ \text{V/cm}$$

where $\nu_c = \xi - \beta$.

Assuming dipole radiation with the above field as the average field, which we take to be the antenna voltage divided by the half-length ($\lambda/4$), with a matched antenna (72-ohm radiation resistance), we have

$$P_{rad} = \frac{V^2}{R_{rad}} = \frac{(E_{rms} \cdot \lambda/4)^2}{72}$$

$$= (E_{rms}\ \lambda)^2/1152$$

$$= 3.3\ \text{MW} \quad . \tag{4.35}$$

To see if the above estimates are reasonable, we examined extrapolated CW breakdown data presented by Scharfman and Morita.[21] They found that a 0.24 λ monopole at 240 MHz broke down at 80 W for a pressure of 3.10^{-2} torr. If we extrapolate to a dipole operated at the same frequency at an altitude of 200 km, the breakdown power is

$$P_{bd} \approx 2 \times 80 \times \left(\frac{0.03}{p}\right)^2 = 2.65 \times 10^{12}\ \text{W} \quad . \tag{4.36}$$

Whitmer and MacDonald[19] also presented results for an effective diffusion length $\Lambda = \lambda/2$ with ambipolar diffusion on a reentry body. The breakdown electric field strength at 120 km was 30 V/cm. Extrapolating to 140 km gives $E_{bd} > 1000$ V/cm, which indicates a higher breakdown power than that computed in this section.

4.7.2. Field-Emission Effects

Field emission refers to the freeing of electrons from the antenna material due to the presence of high electric fields. When the

electric field strength exceeds the surface potential of the antenna material, electrons will be liberated. As a rule of thumb, the required electric field strength is of the order of 10^4 V/cm. If we assume a radiated power of 1 MW, we can estimate the electric field strength around the tip of a dipole where the field is most intense.

For a radiation resistance of 72 Ω, the current is 118 A. Then the electric field at the tip can be computed as follows:

$$E_{tip} = \frac{91\ I(0)}{a \sin kh} \text{ V/cm} \tag{4.37}$$

where

$I(0)$ = Current at the feedpoint

a = Antenna radius = $d/2$, cm

k = $2\pi/\lambda$

h = Half-length of antenna.

Therefore,

$$E_{tip} = \frac{91\ I}{a} \quad . \tag{4.38}$$

If we assume $h/d = 10$, or $a = \lambda/80 = 5/8$ cm, the tip electric field is

$$E_{tip} \sim 17{,}000 \text{ V/cm} \quad . \tag{4.39}$$

Therefore, for a simple half-wavelength dipole with a length-to-diameter ratio of 20, field emission at 1 MW radiated power is important. While techniques exist that can significantly lower the tip electric field strength, it seems clear that field emission must be considered in the specific antenna design used for an antenna for an incoherent-scatter radar on board the Space Shuttle.

4.7.3 Multipactor Discharges

Multipactor discharges are also known as secondary-electron resonance discharges. The classic case is an alternating field between parallel plates, with frequency, plate spacing, and voltage such that at the time when secondary electrons are freed by bombardment at one plate, the field reverses and a larger number of electrons are accelerated to the other plate in time for the reversal again. While this effect is extremely difficult to assess without specific details of the antenna geometry, experimental studies[22] indicate that multipactor breakdown predominates over gas discharge breakdown at low pressures such as that expected around the Space Shuttle.

4.8 Phased-Array Antenna

With antenna breakdown possibly becoming a problem at megawatt peak powers (Section 4.7), we briefly consider the utilization of a phased-array antenna to alleviate this problem. By employing n radiating elements, we can distribute the peak power such that the actual power level applied to each element is 1/n times the total peak power. A further advantage of such an antenna is that it is capable of being implemented so that electronic beam steering becomes a possibility. With electronic beam steering, the steering limitations (in particular, the low slew rate) imposed by the unfurlable reflector antenna discussed in a previous section could be circumvented. With a rapid slew-rate capability, multiple beam-position measurements that are essential for resolving the bulk plasma velocity vector (and hence, the electric field vector) can be made. This capability is of critical importance for a satellite-borne radar traveling at orbital velocities.

In the case of a square planar antenna array with elements spaced half-wavelength apart, its effective aperture, A, is related to the

physical aperture, A_o, by the proportionality factor g/π (i.e., $A = gA_o/\pi$) where g is the gain of each radiating element. This relation assumes that the physical aperture is filled with appropriately spaced radiating elements. To fill a given physical aperture, we will require $4A_o/\lambda^2$ radiating elements. Clearly, we will require a smaller number of elements to fill the physical area at lower frequencies. For this reason, a given effective aperture, or SNR, will be less expensive at lower frequencies.

Another way of viewing the same problem is to compute the SNR as a function of frequency assuming a fixed number of radiating elements. If the number of elements is fixed, the SNR, which is proportional to the effective aperture, takes on an additional λ^2 dependence. The relative SNRs for this case are plotted in Figure 4.9. The three sets of relative SNR curves for a fixed number of radiating elements are shown next to the corresponding set of SNRs for a parabolic reflector (see Figure 2.3). The SNRs corresponding to the space-oriented sector are labeled SNR_s, and those corresponding to the earth-oriented sector are labeled SNR_e.

The SNRs for the earth-oriented sector decrease monotonically as the frequency is increased. On the other hand, the SNRs for the space-oriented sector are relatively constant at the lower frequencies up to approximately 200 MHz. At frequencies above approximately 300 MHz, the SNRs decay with a slope similar to those found for the earth-oriented sector. From this figure, we conclude that the SNR can be optimized for a planar antenna array with a fixed number of radiating elements if the array is operated at frequencies below 300 MHz.

For an array at 300 MHz, we can estimate the maximum number of radiating elements required to fill a physical aperture equal to that of the 183-m (600-ft) diameter parabolic reflector. The physical area of the reflector is 2.6×10^4 m^2. An equivalent square area is $(162\ m)^2$. If we assume that the radiating elements are to be spaced $\lambda/2$ apart, we will require 324 elements to a side, or a total of 105,208 elements to fill the

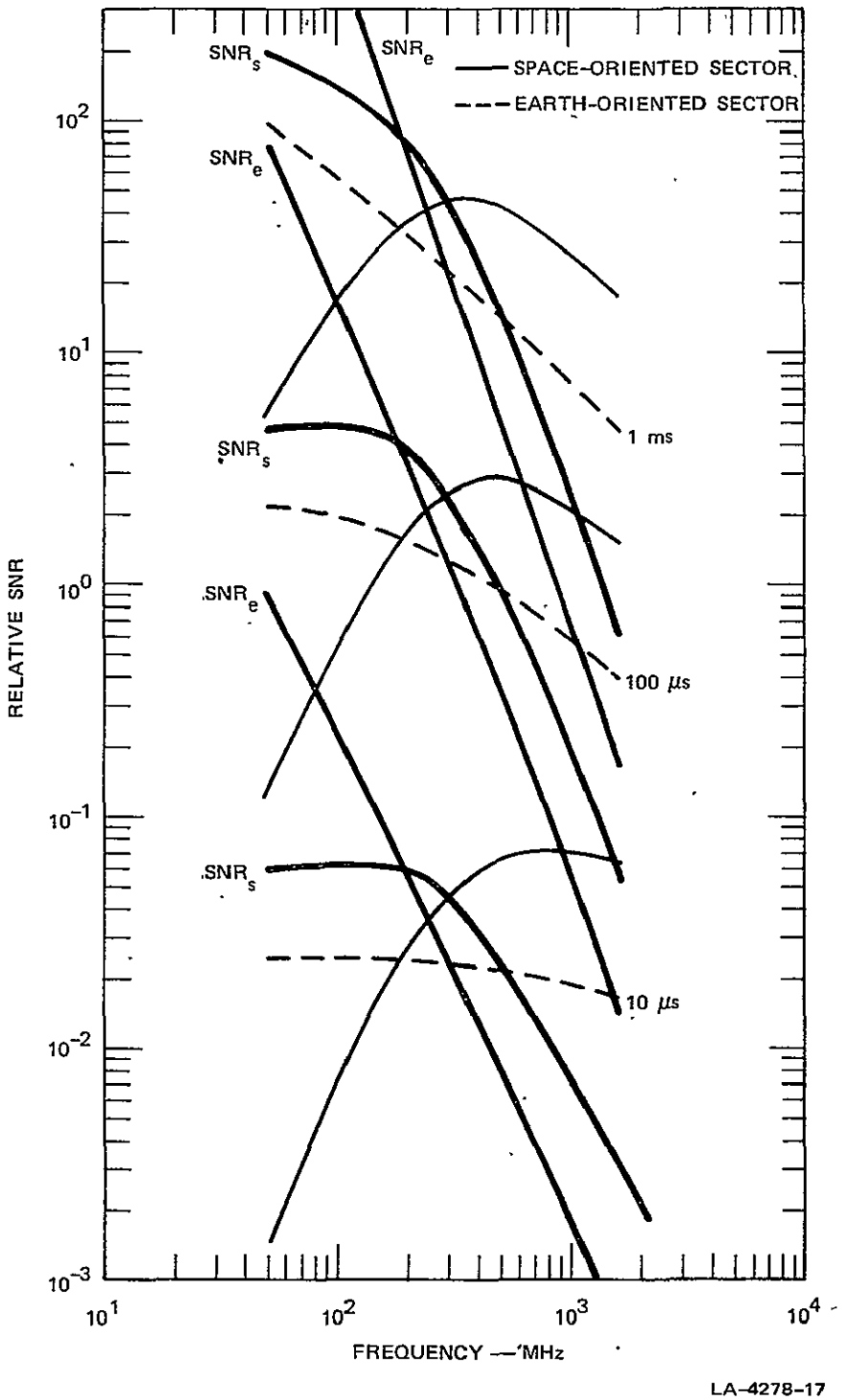

FIGURE 4.9 SNR DEPENDENCE ON λ, τ FOR A FIXED-DIMENSION PHASED-ARRAY ANTENNA

ORIGINAL PAGE IS
OF POOR QUALITY

total area. Since a limited amount of "thinning" of the element distribution does not significantly degrade the antenna performance, we will probably need of the order of 10^5 radiating elements. If we consider operating at 100 MHz, the required number of radiating elements is reduced to 11,664, or of the order of 10^4. If we assume that the cost of the individual elements is constant, the antenna array designed for 100-MHz operation would be an order of magnitude less expensive than that designed for 300-MHz operation.

The selection of a lower operating frequency has repercussions for other radar design parameters. The waveform must be altered to account for the narrower frequency spectrum of the incoherent-scatter signal. In order to resolve the spectrum with a single pulse, the transmitted spectrum must be narrow compared to the incoherent-scatter spectrum. This means the 200-μs pulsewidth, which is appropriate at an operating frequency of 600 MHz, is no longer adequate and that the pulsewidth must be increased to 400 μs at 300 MHz and to 1.2 ms at 100 MHz. Alternatively, the autocorrelation function (ACF) is proportionately stretched out in time, and therefore a minimum lag resolution of 40 μs is required at 300 MHz, and of 120 μs at 100 MHz. Therefore, while the individual pulsewidth in the burst waveform can be arbitrarily selected (but not exceeding 120 μs), their separations in time must be proportionately increased (by a factor of 2 at 300 MHz and a factor of 6 at 100 MHz) from the separations shown in Figure 3.4. Consequently, the single-pulse mode, while adequate for spectral measurements, has a relatively poor range resolution of 60 km at 300 MHz and 180 km at 100 MHz. The burst waveform can still be utilized by varying the individual pulsewidths from 20 to 120 μs. However, the SNR is decreased by a factor no less than 120/200 and the duty cycle is increased by as much as a factor of 720/200.

The decrease in SNR must be accounted for by increasing either the peak power or the antenna aperture. The increase in duty cycle must be

accounted for by increasing the waveform repetition period, which amounts to reducing the spatial resolution along the velocity vector. The increased interpulse spacing within the burst waveform results in a minimum range (see Table 3.1) of 80 km at 300 MHz and 230 km at 100 MHz. Both minimum ranges appreciably reduce the range over which incoherent-scatter measurements can be made.

Since the above waveform analysis is based on achieving adequate spectral resolution, we must conclude that spectral measurements are not practical at these lower operating frequencies. The alternative is to revert to a power-only (i.e., electron density) measurement mode. However, most of the plasma parameters--e.g., electric field, and electron and ion temperatures--are computed through the spectral measurements. Furthermore, as mentioned at the beginning of this subsection, part of the appeal of a phased-array antenna is its rapid beam-positioning capability, which has its most useful application in the electric field measurements.

From the above discussion, it appears that regardless of its cost, a phased-array antenna, if utilized, should be designed and operated at frequencies above 300 MHz.

Although a feasibility study of deploying this type of antenna in space has not been conducted to the authors' knowledge, we would anticipate a multitude of added complexities over and above those associated with the deployment of an unfurlable reflector antenna. The end result may be an antenna with not nearly the physical aperture possible with an unfurlable parabolic reflector. However, since antenna breakdown problems are alleviated with the antenna array, the decreased aperture can probably be compensated for by the use of higher peak powers. A detailed study would have to be conducted to evaluate its feasibility.

Another consideration is the fractional bandwidths associated with phased-array antennas. Because the elements are usually resonant radiators and their mutual spacing is dependent on the operating frequency, 5% would be a typical fractional bandwidth. If frequency shifting up to 20 MHz is to be employed for clutter mitigation, then a higher operating frequency (say, greater than 400 MHz) would be desirable in order that the maximum frequency shift could be made within the fractional bandwidth of the antenna.

5. SEMICOHERENT BACKSCATTER STUDIES

In Section 4.2.3, we briefly discussed the auroral clutter that would be expected when a backscatter radar is operated in space. While E-region clutter that is field-aligned can probably be mitigated by the techniques described in Section 4.2.4 because of its occurrence at ranges comparable to those of ground clutter, F-region clutter may present a more serious problem in that it may very well occur at ranges comparable to the desired incoherent-scatter signal.

Because of the potential seriousness of this problem, and because so little is yet known about field-aligned clutter, we present an overview of this subject in this section. From the discussion, it should become apparent that semicoherent backscatter studies should be performed prior to the development of an incoherent-scatter radar in space. In addition to experimentally determining the impact of clutter on incoherent-scatter measurements, the study would be of interest scientifically, particularly if the field-aligned auroral clutter can be discriminated from ground clutter.

Some of the scientific benefits of such a radar are discussed below. In particular, we focus our attention on the mapping of field-aligned irregularities, the more interesting of which occur in the auroral and polar cap ionospheres.

5.1 E-Region Irregularities

Field-aligned irregularities have been observed in the E region by ground-based VHF-UHF backscatter radars for many years. The studies have been primarily restricted to the equatorial and auroral E regions.

Present understanding is that the production mechanism of these irregularities is some kind of a plasma instability driven by an electric field. More recent evidence obtained with HF radars operated within the polar cap suggests that a similar instability is also operative in the polar cap.[23-25]

5.1.1 Equatorial Backscatter Studies

Ground-based radar backscatter studies at the magnetic equator have produced many of the breakthroughs in this field. The major breakthrough occurred in 1963 when Bowles et al.[26] showed that the radar echoes from the equatorial electrojet displayed characteristics that could be explained only by an angular spectrum of acoustic plasma waves. Buneman[27] and Farley[28] independently developed a two-stream instability model capable of explaining some of the major observational features. In 1969, Balsley[29] identified a second type of irregularity that was clearly not due to the two-stream instability. Since then, these "Type 2" irregularities have been attributed to the gradient-drift instability.[30]

The importance of the discovery of Type 2 irregularities is that the associated mean Doppler velocity appeared to be directly related to the electron drift velocity.[29,31] Furthermore, if the characteristic near-constant Doppler velocity (observed as a function of the angle between the electron drift velocity and the radar viewing angle) of the radar backscatter from Type 1 (or two-stream) irregularities can be attributed to the ion-acoustic speed, it is then possible to extract the electron and ion temperatures from this measurement.[31]

There is no obvious advantage in studying the equatorial electrojet irregularities from a satellite. It is restricted in latitude, well-behaved, and best studied by continued ground-based experiments. In contrast, similar irregularities found in the auroral and polar cap regions

are widespread geographically, dynamic in behavior, and best characterized by a scanning backscatter radar on a satellite.

5.1.2 Auroral Backscatter Studies

Scanning radars in the auroral zone[9,32-35] revealed that a Doppler-velocity variation with radar viewing angle relative to the current direction existed that was analogous to those found at the equator. Tsunoda[35,36] showed that these auroral echoes could not be produced by primary plasma waves generated by the two-stream instability. On the other hand, he showed that the azimuth at which the Doppler shift changed from a negative sign to a positive sign corresponded to the direction perpendicular to the current flow. Furthermore, he showed that the slope of the Doppler-velocity variation appeared to be proportional to the electron drift velocity. Regions of near-constant Doppler velocity as a function of azimuth were also observed in directions more along the current flow,[34-36] analogous to the observations at the equator.

Recent studies of the radar aurora have indicated that the backscatter amplitude characteristics provide a measure of mean ionospheric plasma parameters. Greenwald et al.[37,38] showed that the range-integrated amplitude of the diffuse radar aurora is linearly proportional to perturbations of the horizontal component of the geomagnetic field as measured by a magnetometer located beneath the scattering region. The results imply a direct correspondence between the backscattered amplitude and the E-region current density. Tsunoda and Presnell[39] showed that the occurrence of 398-MHz diffuse auroral echoes is associated with a nominal threshold electric field strength of 30 mV/m. That is, when the electric field strength exceeds that value, auroral echoes are observed and, when the electric field strength is below that value, the auroral echoes are not observed, regardless of the mean electron density. Therefore, the occurrence of 398-MHz diffuse auroral echoes can be used as a measure of the presence of enhanced electric field in that vicinity.

The usefulness of rapid spatial scans of the auroral clutter was first demonstrated by Tsunoda et al.[40] Using a phased-array radar operated at 398 MHz, they showed that the radar aurora, hitherto an enigma in terms of its exact relationship to auroral processes, is in fact one of the more useful means of studying the auroral electrojet characteristics. For example, Tsunoda et al.[40,41] showed that the evening diffuse radar aurora was essentially collocated with the eastward electrojet. Visual auroral arcs were invariably found on the poleward side of the diffuse radar aurora, within the westward electrojet region. From their results, Tsunoda et al.[41] concluded that the poleward boundary of the evening diffuse radar aurora represented the lower latitudinal boundary of the Harang discontinuity.[42] Tsunoda et al.[43] further showed that the evening diffuse radar aurora (and hence, the eastward electrojet) was also collocated with downward field-aligned currents. Rapid two-dimensional mapping of the radar aurora was also shown to be valuable in identifying radar substorm signatures, especially those associated with rapid east-west motions.[44]

It is clear from the above discussion that radar auroral echoes represent a valuable means of studying auroral electrojet behavior. There is currently no other technique capable of mapping the spatial distribution of the auroral electrojets. Its potential value as a satellite-borne experiment is clearly demonstrated in Figure 4.2 (Section 4.2.3). From that figure, we see that the longitudinal coverage is greatly expanded (by approximately a factor of 3) in comparison to the coverage possible with a ground-based radar. Furthermore, by the use of the polar orbit of the satellite, complete latitudinal coverage of both the auroral and polar cap region is possible. However, a means must be found to minimize the effects of ground clutter (see Section 4.2).

5.1.3 Polar Cap Backscatter Studies

The presence of plasma instabilities in the polar cap E region has only recently been recognized. Olesen[23] proposed that the slant-E echo trace[45] observed in polar cap ionograms was due to direct backscatter from field-aligned irregularities generated by the Buneman-Farley two-stream instability. Support for this hypothesis was given by a number of workers. Mozer et al.[46] showed that the average polar cap electric field strength was 30 mV/m. Such an electric field strength is clearly above the threshold electric field required by the two-stream instability.[27,28] Other tests have been made of the relationship between the occurrence of the slant-E echo (or its associated "slant-E condition," or SEC) and the electric field strength.[24,47,48] Tsunoda et al.[25] showed that the azimuthal distribution of slant-E echoes was related to the direction of the polar cap electric field, which is also consistent with a plasma instability as the driving mechanism of slant-E echoes.

The reason that plasma-instability-related echoes are observed in the polar cap at HF and not at higher frequencies (i.e., not above, say, 40 MHz) is the magnetic-aspect requirements. Significant backscatter is produced only when the radar signal is incident at nearly right angles with the geomagnetic field. At HF frequencies, ionospheric refraction allows this condition to be satisfied. Therefore, it is anticipated that with a UHF scanning radar on board the Space Shuttle, we will for the first time be able to study in a comprehensive manner the polar cap electric fields and currents through the backscatter characteristics.

The large-scale mapping of enhanced electric field regions by a scanning radar in space holds most appeal in the polar cap region. Except for the incoherent-scatter radar, there are no existing ground-based techniques that are capable of measuring the electric field distribution in the polar cap. Because of its high cost, the deployment of a

network of incoherent-scatter radars is prohibitive. Even if an inexpensive ground-based technique is developed in the near future, the deployment of a dense network of such stations would be difficult due to the remoteness of the polar cap region. At present, the only available means of mapping electric fields in the polar cap region are in situ measurements by balloons, rockets, and satellites. Yet all these techniques as well as the incoherent-scatter radar on the Space Shuttle make either point measurements or, at best, one-dimensional measurements (e.g., a map of the electric field in latitude for a given longitude). In comparison to the above measurement techniques, a polar-orbiting backscatter radar is capable of providing two-dimensional mapping of the entire polar cap with each orbit (i.e., of the order of 100 minutes). Coverage of the entire polar cap can be clearly seen by comparing the longitudinal width of the annular magnetic aspect contours for a satellite at 65° geographic latitude (see Figure 4.2) to the diameter of the polar cap region (which is, say, bounded by 75° geographic latitude).

5.2 F-Region Irregularities

Another region in which field-aligned backscatter might be significant is in the auroral F region. As with the polar cap region, magnetic-aspect requirements cannot be easily satisfied by typical ground-based radars. However, UHF auroral echoes have been observed by Leadabrand et al.[32] up to an altitude of 160 km or so, which was the maximum height at which orthogonality was achieved. Schlobohm et al.,[33] operating a VHF radar at 43° geomagnetic latitude, observed auroral echoes up to an altitude of 300 km during several intense auroral events.

Theoretical support for the probable existence of F-region auroral echoes was recently presented by Ott and Farley.[49] They showed that microinstabilities would be expected to be operative in the auroral F region when the electric field strengths exceeded about 50 mVm. Of the various

instabilities that might occur, they showed that the Post-Rosenbluth instability[50,51] was by far the most important. The instability threshold conditions require that the ion drift velocity (equal to E/B in the F region) exceed 1.8 times the thermal velocity of the neutrals. When this condition is met, growing plasma waves are generated that propagate nearly perpendicular to the geomagnetic field. Their theory predicts that the fastest growing mode will occur at a corresponding radar frequency of 1 to 2 GHz. However, as the instability is driven harder, the corresponding frequency decreases. It is clear even from the limited observations that F-region field-aligned clutter can occur at frequencies as low as 100 MHz.[33]

In addition to the magnetic-aspect limitations of ground-based radars, the geometry of the radar viewing angle with respect to the electric field vector is also important. In order to observe the primary plasma waves generated by this instability, the radar beam must be pointed in a direction in which the component of the ion-velocity vector exceeds the threshold velocity. Therefore, it is clear that the radar viewing angle cannot be along the electric field vector. However, as seen, for example, in Figure 4.2, ground-based radars must look in a generally northerly direction to satisfy the magnetic-aspect requirement. In other words, a substantial east-west electric field component is required in order for the ground-based radar to observe the F-region auroral echoes. In general, the east-west electric field component as found in the auroral zone is small compared to the north-south electric field component, and is usually less than 50 mV/m. Therefore, most of the F-region (as well as E-region) auroral echoes observed by ground-based radars are probably associated with secondary plasma waves. If this is the case, the amplitude of the secondary waves is probably significantly smaller than that of the primary plasma waves.

On the other hand, we see from Figure 4.2 that a satellite-borne radar is located within the magnetic aspect contours. Consequently, orthogonality can be satisfied at all azimuths. Therefore, regardless of the direction of the electric field vector, the satellite-borne radar will always be able to detect the primary plasma waves associated with this instability. The clutter amplitude associated with the primary waves may be significantly greater, for example, than the estimates made by Jaye et al.[8] using a ground-based radar.

6. DISCUSSION

A detailed yet preliminary study has been completed, evaluating the feasibility of an incoherent-scatter radar aboard the Space Shuttle. At the outset, it was clear that because an incoherent-scatter radar is capable of comprehensive plasma measurements that are not possible with other techniques, the operation of such a radar from the Space Shuttle should be scientifically rewarding. Therefore, its scientific value was not in doubt, but the question whether it would represent a practical, cost-effective experiment was evaluated. It seems clear from the findings presented in this report that it is technically feasible to conduct such an experiment. Since its feasibility does not imply a totally flexible system comparable to ground-based incoherent-scatter radars, we summarize its limitations.

For a typical Space Shuttle orbit at an altitude of 400 km, the maximum desirable range is approximately 300 km. At that range, the ionosphere from 100 to 700 km altitude could be probed by the radar. If the maximum usable range was limited to 100 km, the radar would be limited to F-region measurements unless the orbit altitude is altered. Assuming that a 183-m-diameter antenna was available for Space Shuttle use, the SNR using 1 MW peak power at 600 MHz would range from 0.5 (space-oriented sector) to 0.15 (earth-oriented sector) at a range of 300 km. These estimates are based on a pulsewidth of 20 μs and an electron density of 10^{11} el/m^3. This electron density value is typical of a sunlit E layer or the density that exists during moderate auroral activity.[51] This means that E-region electron densities under quiet nighttime conditions cannot be accurately measured with a 20-μs pulse. However, it can be measured with less range resolution by utilizing the 200-μs pulsewidth.

The specified 1-MW peak power can be achieved in principle by reducing the duty cycle of the transmitter. Two problems arise when this is done. First, at a 1-MW peak power, problems of antenna breakdown may become significant. However, a more definitive study of specific antenna designs is required before the seriousness of these problems can be evaluated. An alternative antenna design that circumvents the breakdown problem is a phased-array antenna. And second, the reduction in the duty cycle amounts to a corresponding reduction in spatial resolution due to the need for longer integration times. For 1-MW peak power and 200-μs pulsewidth, it would take 107 s to collect 400 samples. This integration time amounts to a spatial resolution along the velocity vector of 850 km. Therefore, if 1-MW peak power is necessary, the average power limitation imposed by the Space Shuttle must be alleviated, possibly by the use of an energy-storage device. Depending on the required capacity of such a device, its weight might pose another problem.

Assuming that the duty cycle can be arbitrarily increased by the use of an energy-storage device, the sampling rate will be limited by the presence of ground clutter, both in the mainlobe and sidelobes of the antenna. The simplest scheme for clutter mitigation is to vary the waveform repetition period such that the desired signal does not occur at the same range as the ground clutter. This kind of scheme would limit the repetition period to approximately 15 ms. With this sampling rate, the spatial resolution (along the velocity vector), assuming that 400 samples are required, is 48 km. The sampling rate, and hence the spatial resolution, can be further improved by utilizing a frequency-shift technique, which may be desirable when the 20-μs pulse-burst waveform is used.

Another type of clutter that is potentially more damaging to incoherent-scatter measurements than ground clutter is F-region auroral clutter. If it is operative, the clutter can occur at ranges comparable to those of the incoherent-scatter signal, making it virtually impossible

to discriminate against the clutter. Since the existence of this clutter has already been predicted theoretically but cannot be easily verified experimentally by ground-based radars, it would be highly desirable to conduct a backscatter radar experiment from a spacecraft to determine the extent of the clutter environment.

7. RECOMMENDATIONS FOR FUTURE STUDY

A number of outstanding problems remain to be investigated before definite conclusions can be drawn regarding the feasibility of performing an incoherent-scatter radar experiment on board the Space Shuttle. The areas requiring further study are summarized below.

Ground and F-region auroral clutter remains a potentially serious problem. The clutter problem should be reexamined in more detail. One approach would be to model the ground clutter more accurately. Computer simulation of ground and sea reflectivity as a function of frequency, terrain features, sea state, and other variables would shed more light on the severity of this problem. Specific antenna designs should also be considered as a means of suppressing the sidelobes.

Auroral clutter characteristics as observed from the Space Shuttle should be modeled on the basis of both the auroral and polar cap ionospheres. Means of discriminating ground clutter from auroral clutter should be investigated as well as mitigation against its effects on incoherent-scatter measurements. Doppler processing may be a means of discriminating auroral clutter from ground clutter.

Because so little is known about the mechanisms that produce auroral clutter, it would be highly desirable to conduct satellite-borne radar experiments to determine the extent of the auroral clutter environment in space. In addition to defining the clutter environment in which the incoherent-scatter radar must operate, the data collected by such experiments can be potentially rewarding from a scientific point of view (see Section 5).

PRECEDING PAGE BLANK NOT FILMED

Further studies are needed to model and quantify the antenna breakdown problem. Until specific antenna configurations are considered, little, if any, can be said about the seriousness of multipactor breakdown. These studies would influence the choice of antenna for deployment in space.

The deployment of phased-array antennas of any size in space has, to date, not been investigated. The feasibility and associated costs of such deployment would have to be evaluated in the light of results obtained from the above recommended studies.

It appears that if an incoherent-scatter radar having the flexibility of comparable ground-based systems is desired, a means of efficient energy storage must be found. In this case, weight and volume per unit energy stored is a primary factor.

Finally, the problem of dissipating the heat generated by high-power transmitters has to be investigated. This problem was not approached in this preliminary feasibility study.

REFERENCES

1. J. V. Evans, "Theory and Practice of Ionosphere Study by Thomson Scatter Radar," Proc. IEEE, Vol. 57, p. 496 (1969).

2. R. L. Leadabrand, M. J. Baron, J. Petriceks, and H. F. Bates, "Chatanika, Alaska, Auroral Zone Incoherent-Scatter Facility," Radio Sci., Vol. 7, p. 747 (1972).

3. F. W. Crawford, "Plasma Wave and Resonance Phenomena," presented at AIAA 13th Aerospace Sciences Meeting, Pasadena, California January 20-22, 1975.

4. T. N. Davis, "Scientific Design of a Manned Aurora and Magnetosphere Observatory System for the Shuttle Program," Final Report, Vols. I and II, Contract NAS 9-72649, Geophysical Institute, University of Alaska (February 1973).

5. G.K.C. Campbell and J. B. Damonte, "Large Deployable Antenna Forecast: 1975-2000," LMSC-D384788, Lockheed Missiles and Space Company, Inc., Sunnyvale, Calif. (December 1974).

6. D. T. Farley, "Multiple/Pulse Incoherent Scatter Correlation Function Measurements," Radio Sci., Vol. 7, p. 661 (1972).

7. M. I. Skolnik, Introduction to Radar Systems, p. 522 (McGraw-Hill Book Co., New York, N.Y., 1962).

8. W. E. Jaye, W. G. Chesnut, and B. Craig, "Analysis of Auroral Data from the Prince Albert Radar Laboratory," Final Report, Contract 601932 under DA-30-30-069-AMC-333(Y), SRI Project 7465, Stanford Research Institute, Menlo Park, California (September 1969).

9. W. G. Chesnut, J. C. Hodges, and R. L. Leadabrand, "Auroral Backscatter Wavelength Dependence Studies," Final Report, Contract AF 30(602)-3734, SRI Project 5535, Stanford Research Institute, Menlo Park, California (June 1968).

10. Spacelab Payload Accommodation Handbook, NASA/ESRO/CERS, ESTEC Ref. No. SLP/2104, George C. Marshall Space Flight Center, Huntsville, Ala. (October 1974).

11. Space Shuttle System Payload Accommodations. Level II. Program Definition and Requirements, Vol. XIV, NASA/JSC, Houston, Texas (July 3, 1974).

12. Personal communication with George K. C. Campbell of Lockheed Missiles and Space Company (1975).

13. T. Geyling and H. Westerman, Introduction to Orbital Mechanics, pp. 118-121 (Addison-Wesley Publ. Co., Reading, Mass., 1971).

14. F. S. Johnson, Satellite Environment Handbook, 2nd ed. Table 1-3 (Stanford University Press, Stanford, Calif., 1965).

15. M.W.J. Bell, "Space Shuttle Payload Design and Operations Engineering 805.12, Description of the Space Shuttle System," Rockwell International, Downey, Calif. (May 1975).

16. W. C. Taylor, W. E. Scharfman, and T. Morita, "Voltage Breakdown of Microwave Antennas," Advances in Microwaves, Vol. 7, p. 59 (1971).

17. P. B. Bisbing, D. L. McMenamin, A. K. Jordan, and P. M. Scherer, "Study to Obtain Design Data for Reentry ECM Antenna Systems," GE Report No. 68SD591, General Electric Co., Philadelphia, Penn. (1968).

18. W. P. Allis, and D. J. Rose, "The Transition from Free to Ambipolar Diffusion," Phys. Rev., Vol. 93, p. 84 (1954).

19. R. F. Whitmer and A. D. MacDonald, "R.F. Antenna Breakdown Conditions in the Presence of the Plasma Sheath," Planet Space Sci., Vol. 6, No. 149 (1961).

20. U.S. Standard Atmosphere, 1962, prepared under sponsorship of NASA, U.S.A.F., U.S. Weather Bureau (U.S. Government Printing Office, Washington, D.C., December 1962).

21. W. E. Scharfman and T. Morita, "Power-Handling Capability of Antennas, at High Altitude," presented at Plasma Sheath Symposium, Boston, Mass., 7-9 Dec. 1959, published in Electromagnetic Radiation in Hypersonic Environment, Pergamon Press, 1960.

22. G. August and J. B. Chown, "Power-Handling Capability of Radiating Systems in the Exoatmosphere," Final Report, Contract ESO-TR-69-107, SRI Project 5609, Stanford Research Institute, Menlo Park, Calif. (April 1969).

23. J. K. Oleson, "On the Polar Slant E Condition, its Identification, Morphology and Relationship to Other Electrojet Phenomena," in Radar Propagation in the Arctic, J. Frihagen, ed., AGARD-CP-97, Paper No. 27 NATO (1972).

24. F. Primdahl, J. E. Olesen, and F. Spangslev, "Backscatter from a Postulated Plasma Instability in the Polar Cap Ionosphere and the Direct Measurement of a Horizontal E Region Current," J. Geophys. Res., Vol. 79, p. 4262 (1974).

25. R. T. Tsunoda, P. D. Perreault, and J. C. Hodges, "Azimuthal Distribution of HF Slant-E Echoes and its Relationship to the Polar Cap Electric Field," submitted to J. Geophys. Res., 1975.

26. K. L. Bowles, B. B. Balsley, and R. Cohen, "Field-Aligned E-Region Irregularities Identified with Acoustic Plasma Waves," J. Geophys. Res., Vol. 68, p. 2485 (1963).

27. O. Buneman, "Excitation of Field-Aligned Sound Waves by Electron Streams," Phys. Rev. Lett., Vol. 10, p. 285 (1963).

28. D. T. Farley, "A Plasma Instability Resulting in Field-Aligned Irregularities in the Ionosphere," J. Geophys. Res., Vol. 68, p. 6083 (1963).

29. B. B. Balsley, "Some Characteristics of Non-Two-Stream Irregularities in the Equatorial Electrojet," J. Geophys. Res., Vol. 74, p. 2333 (1969).

30. R. N. Sudan, J. Akinrimisi, and D. T. Farley, "Generation of Small-Scale Irregularities in the Equatorial Electrojet," J. Geophys. Res., Vol. 78, p. 240 (1973).

31. R. Cohen, "Phase Velocities of Irregularities in the Equatorial Electrojet," J. Geophys. Res., Vol. 78, p. 2222 (1973).

32. R. L. Leadabrand, J. C. Schlobohm, and M. J. Baron, "Simultaneous Very High Frequency and Ultra High Frequency Observations of the Aurora at Fraserburgh, Scotland," J. Geophys. Res., Vol. 70, p. 4235 (1965).

33. J. C. Schlobohm, R. L. Leadabrand, R. B. Dyce, L. T. Dolphin, and M. R. Berg, "High-Altitude 106.1-Mc Radio Echoes from Auroral Ionization Detected at a Geomagnetic Latitude of 43°," J. Geophys. Res., Vol. 64, p. 1191 (1959).

34. W. G. Abel, and R. E. Newell, "Measurements of the Afternoon Radio Aurora at 1295 MHz," J. Geophys. Res., Vol. 74, p. 231 (1969).

35. R. T. Tsunoda, "Electric Field Measurements Above a Radar Scattering Volume Producing 'Diffuse' Auroral Echoes," J. Geophys. Res., Vol. 80, p. 4297 (1975).

36. R. T. Tsunoda, "Doppler Velocity Maps of the Diffuse Radar Aurora," J. Geophys. Res., Vol. 81, p. 425 (1976).

37. R. A. Greenwald, W. L. Ecklund, and B. B. Balsley, "Auroral Currents, Irregularities, and Luminosity," J. Geophys. Res., Vol. 78, p. 8193 (1973).

38. R. A. Greenwald, W. L. Ecklund, and B. B. Balsley, "Radar Observations of Auroral Electrojet Currents," J. Geophys. Res., Vol. 80, p. 3635 (1975).

39. R. T. Tsunoda and R. I. Presnell, "On a Threshold Electric Field Associated with the 398-MHz Diffuse Radar Aurora," J. Geophys. Res., Vol. 81, p. 88 (1976).

40. R. T. Tsunoda, R. I. Presnell, and R. L. Leadabrand, "Radar Auroral Echo Characteristics as Seen by a 398-MHz Phased-Array Radar Operated at Homer, Alaska," J. Geophys. Res., Vol. 79, p. 4709 (1974).

41. R. T. Tsunoda, R. I. Presnell, Y. Kamide, and S.-I. Akasofu, "Relationship of Radar Aurora, Visual Aurora and Auroral Electrojet in the Evening Sector," submitted to J. Geophys. Res., 1975.

42. J. P. Heppner, "Electric Field Variations During Substorms: OGO-6 Measurements," Planet. Space Sci., Vol. 20, p. 1475 (1972).

43. R. T. Tsunoda, R. I. Presnell, and T. A. Potemra, "The Spatial Relationship Between the Evening Radar Aurora and Field-Aligned Currents," submitted to J. Geophys. Res., 1975.

44. R. T. Tsunoda, and E. J. Fremouw, "Radar Studies of Fast Auroral Forms," Final Report, Contract F44620-73-C-0051, SRI Project 2514, Stanford Research Institute, Menlo Park, Calif. (May 1975).

45. H. F. Bates, "The Slant E_s Echo--a High Frequency Auroral Echo," J. Geophys. Res., Vol. 66, p. 447 (1961).

46. F. S. Mozer, W. D. Gonzalez, F. Bagott, M. C. Kelley, and S. Schultz, "High-Latitude Electric Fields and the Three-Dimensional Interaction Between the Interplanetary and Terrestrial Magnetic Fields," J. Geophys. Res., Vol. 79, p. 56 (1974).

47. J. K. Olesen, F. Primdahl, F. Spangslev, and N. D'Angelo, "On the Farley Instability in the Polar Cap E. Region," J. Geophys. Res., Vol. 80, p. 696 (1975).

48. I. B. Iversen, N. D'Angelo, and J. K. Olesen, "Further Evidence for the Farley-Buneman Instability in the Polar Cap Ionosphere," J. Geophys. Res., Vol. 80, p. 3713 (1975).

49. E. Ott and D. T. Farley, "Microinstabilities and the Production of Short-Wavelenth Irregularities in the Auroral F Region," J. Geophys. Res., Vol. 80, p. 4599 (1975).

50. M. N. Rosenbluth and R. F. Post, "High-Frequency Electrostatic Plasma Instability Inherent to 'Loss-Cone' Particle Distributions," Phys. Fluids, Vol. 8, p. 547 (1965).

51. R. F. Post and M. N. Rosenbluth, "Electrostatic Instabilities in Finite Minor Confined Plasmas," Phys. Fluids, Vol. 9, p. 730 (1966).

55

4 of CB8-31346 FR 1

UNIVERSITY OF CALIFORNIA, BERKELEY

BERKELEY • DAVIS • IRVINE • LOS ANGELES • RIVERSIDE • SAN DIEGO • SAN FRANCISCO SANTA BARBARA • SANTA CRUZ

SPACE SCIENCES LABORATORY
TWX: UC SPACE BERK
(910) 366-7945

BERKELEY, CALIFORNIA 94720

May 27, 1976

Distribution:

Code AS21-D, MSFC
Code AT, MSFC
Code PS01, MSFC (21 copies)
E. Harper, MSFC
W. J. McKinney, MSFC
E. Keith, UCB
SSL Reports

Enclosed please find Figures and Tables which were inadvertently omitted from the final report for NASA Contract NAS 8-31346.

Sincerely,

Forrest Mozer

Forrest Mozer
Principal Investigator

fm;c

Encl.

COMPUTER GENERATION OF A BACKSCATTERED SPECTRUM

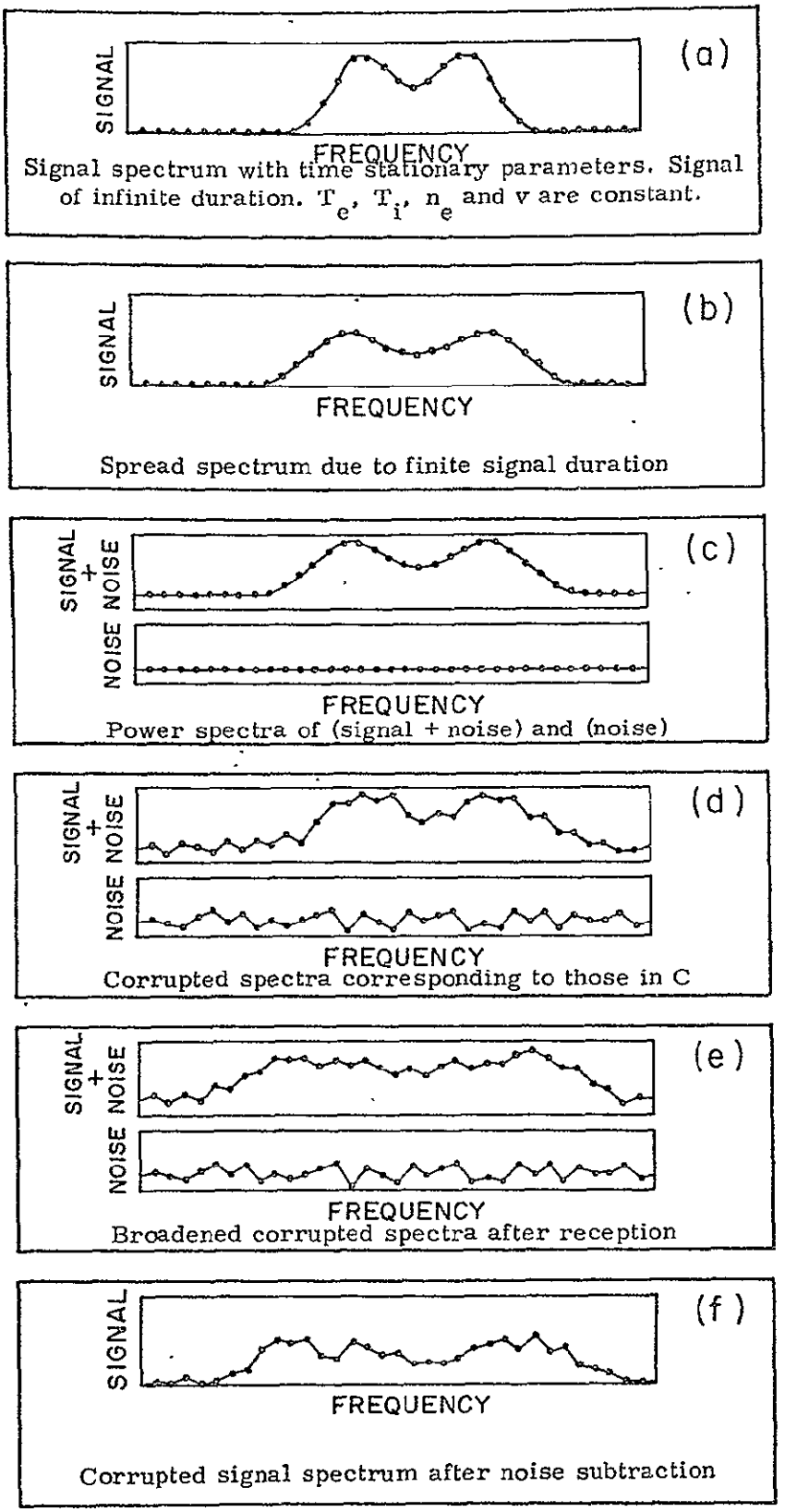

Figure 1

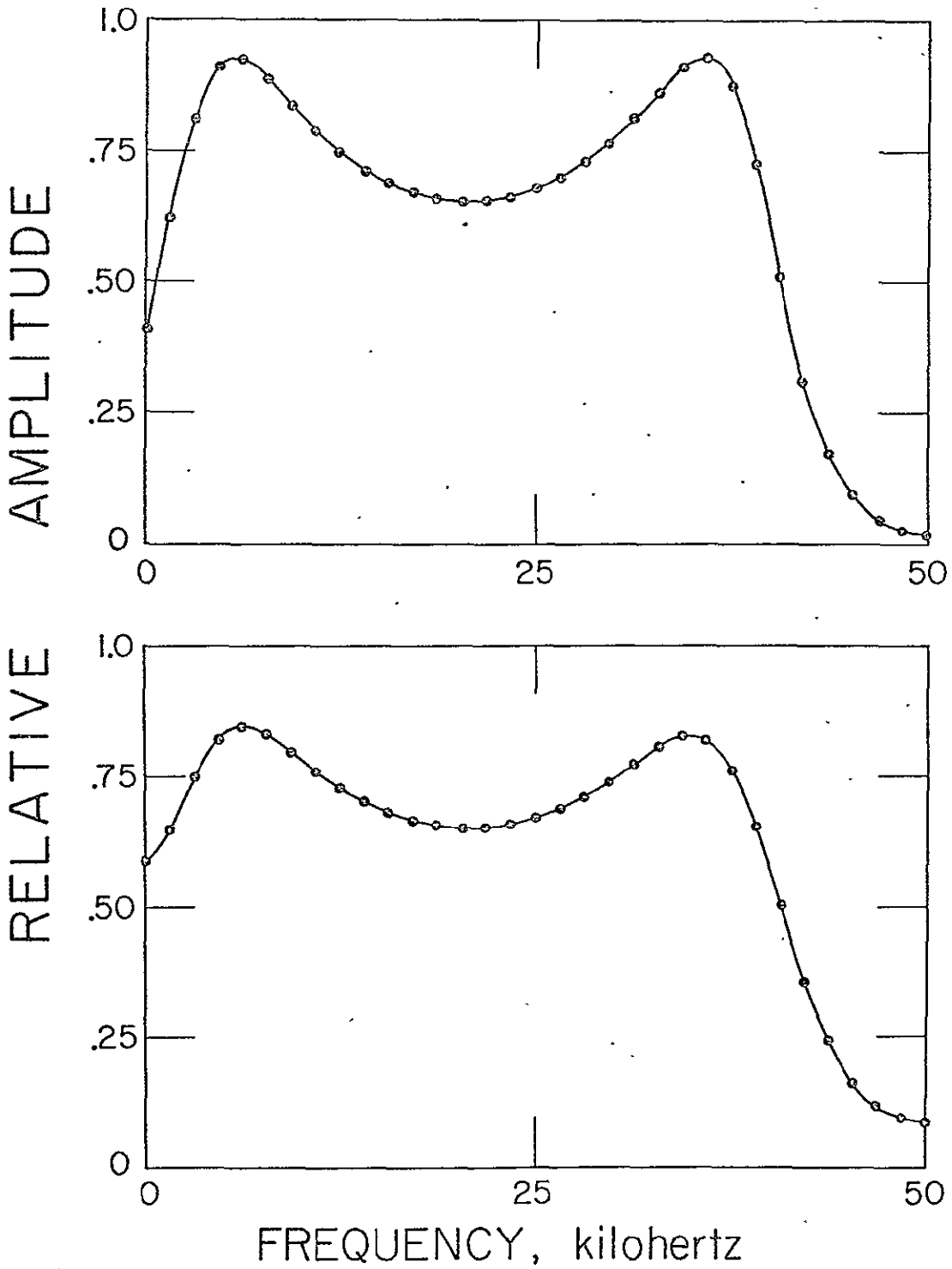
1.0
.75
.50
.25
0
AMPLITUDE
0
25
50
1.0
.75
.50
.25
0
RELATIVE
0
25
50
FREQUENCY, kilohertz

Figure 2

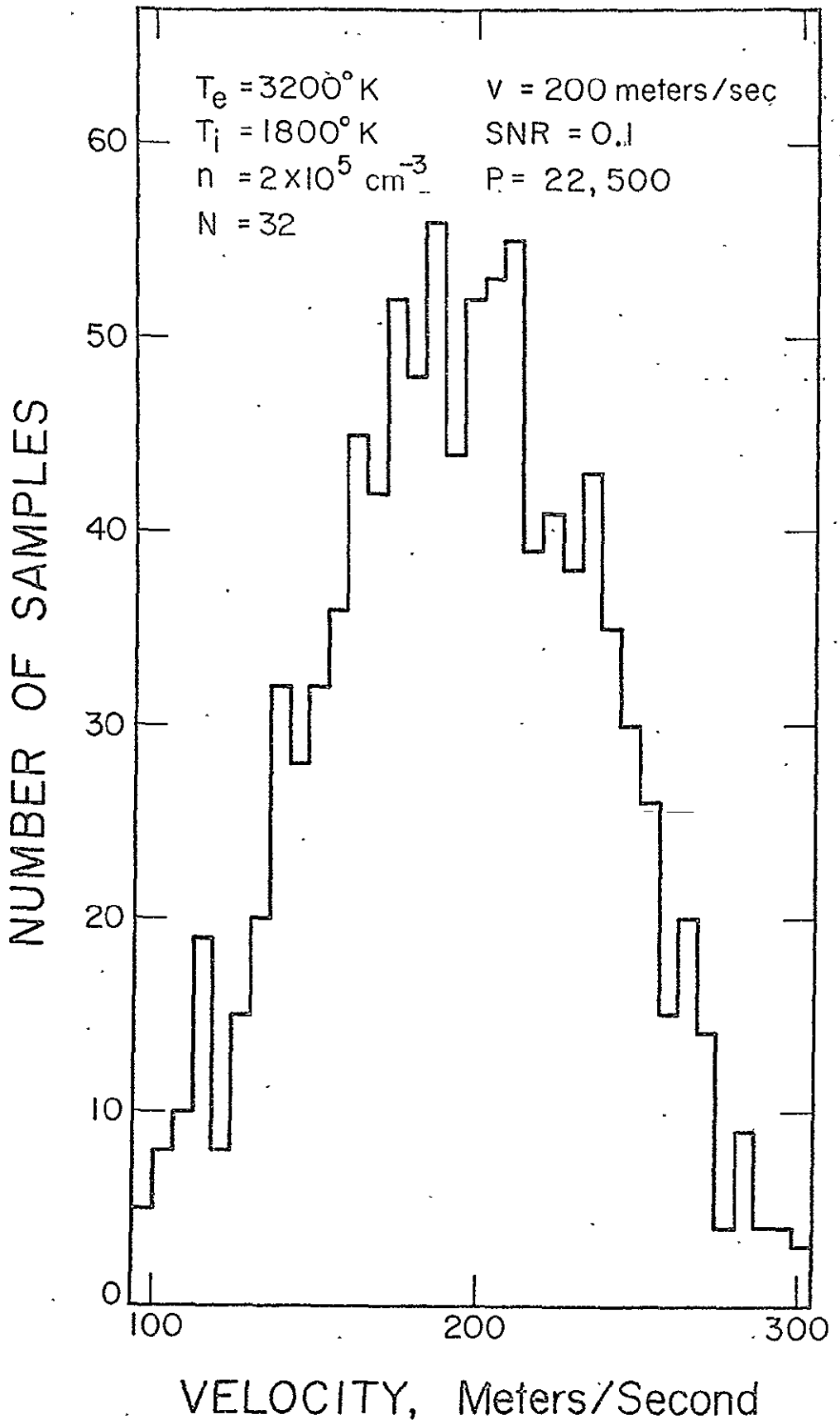
T_e = 3200° K
T_i = 1800° K
n = 2 X 10^5 cm^{-3}
N = 32
V = 200 meters/sec
SNR = 0.1
P = 22,500
NUMBER OF SAMPLES
0
10
20
30
40
50
60
100
200
300
VELOCITY, Meters/Second

Figure 4

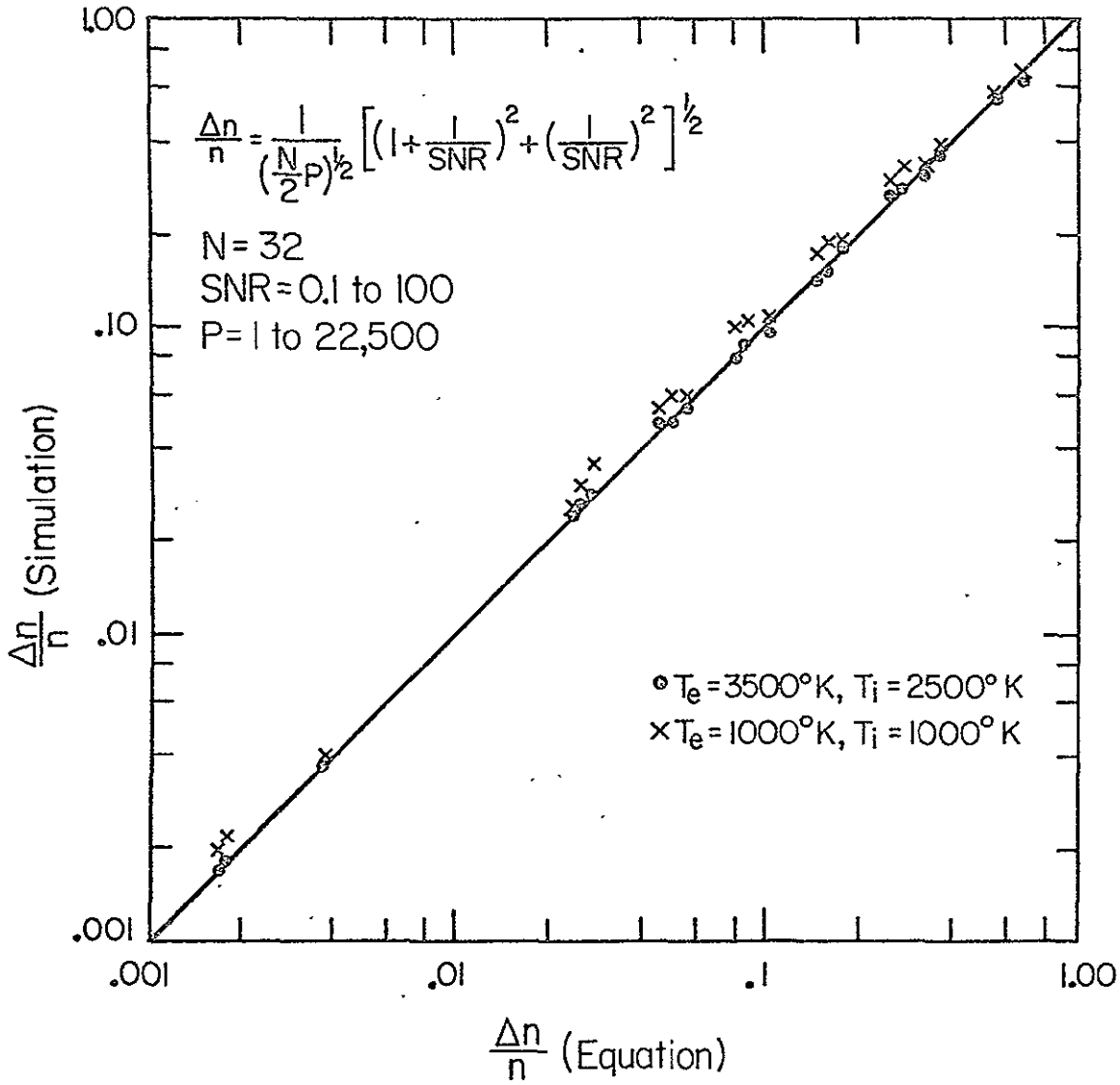
$\frac{\Delta n}{n} = \frac{1}{(\frac{N}{2}P)^{1/2}}\left[\left(1+\frac{1}{SNR}\right)^2+\left(\frac{1}{SNR}\right)^2\right]^{1/2}$
N = 32
SNR = 0.1 to 100
P = 1 to 22,500
T_e = 3500° K, T_i = 2500° K
T_e = 1000° K, T_i = 1000° K
1.00
.10
.01
.001
.001
.01
.1
1.00
$\frac{\Delta n}{n}$ (Simulation)
$\frac{\Delta n}{n}$ (Equation)

Figure 5

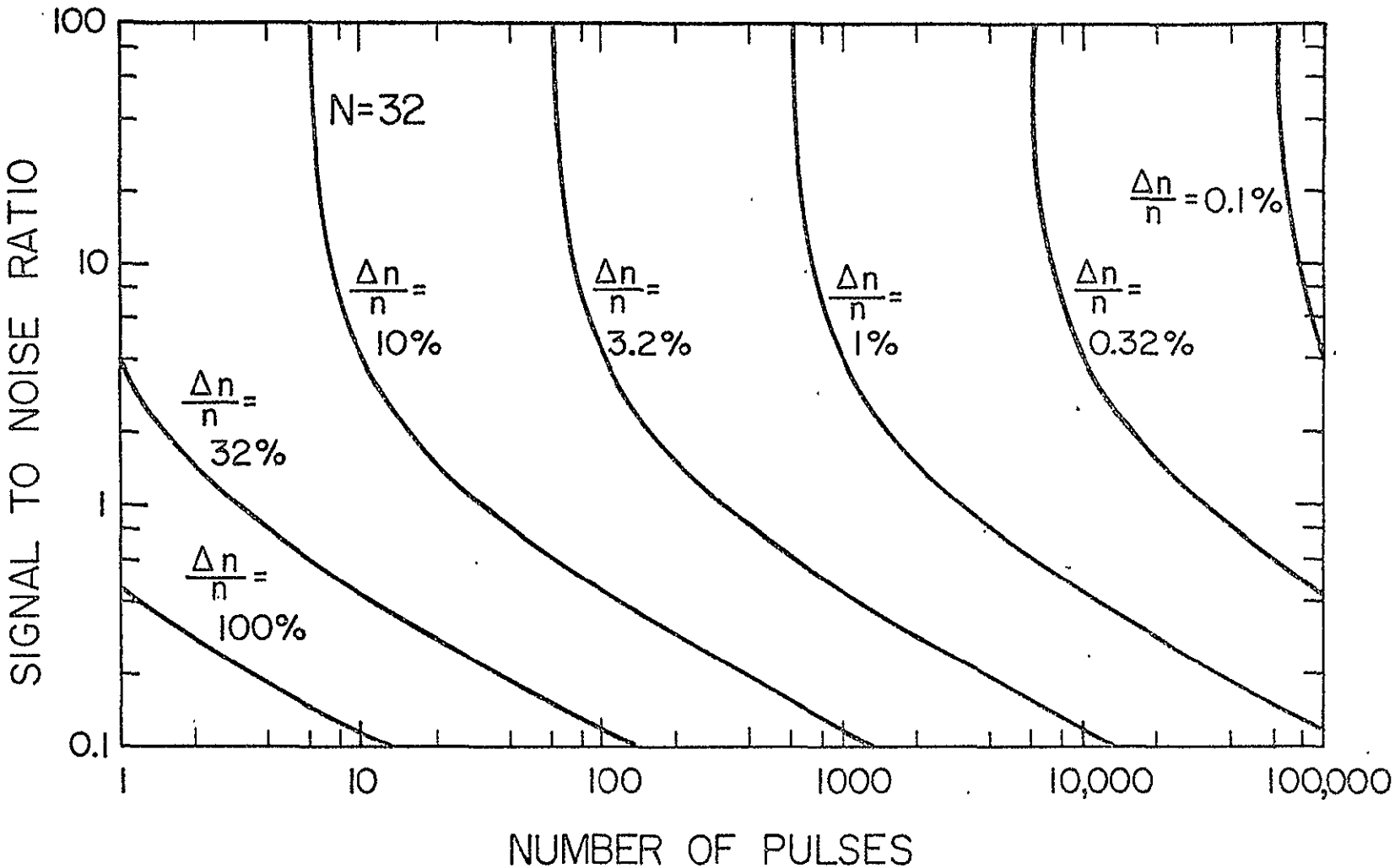
100
10
1
0.1
SIGNAL TO NOISE RATIO
N=32
Δn/n = 10%
Δn/n = 3.2%
Δn/n = 1%
Δn/n = 0.32%
Δn/n = 0.1%
Δn/n = 32%
Δn/n = 100%
1
10
100
1000
10,000
100,000
NUMBER OF PULSES

Figure 6

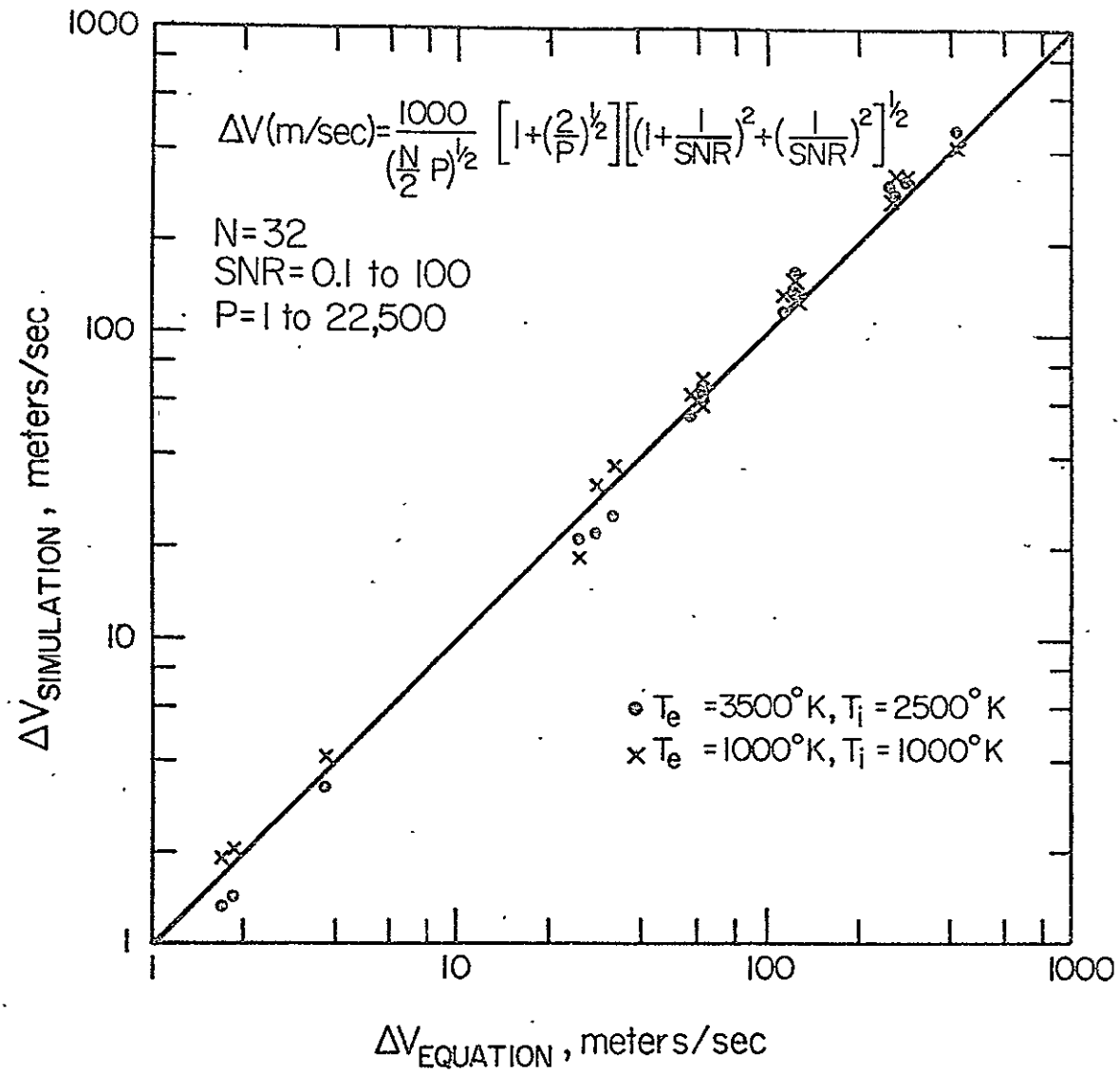
$\Delta V(m/sec) = \frac{1000}{(\frac{N}{2}P)^{1/2}} \left[1+(\frac{2}{P})^{1/2}\right]\left[(1+\frac{1}{SNR})^2+(\frac{1}{SNR})^2\right]^{1/2}$
N=32
SNR=0.1 to 100
P=1 to 22,500
T_e =3500°K, T_i = 2500°K
T_e =1000°K, T_i = 1000°K
1000
100
10
1
1
10
100
1000
$\Delta V_{SIMULATION}$, meters/sec
$\Delta V_{EQUATION}$, meters/sec

Figure 7

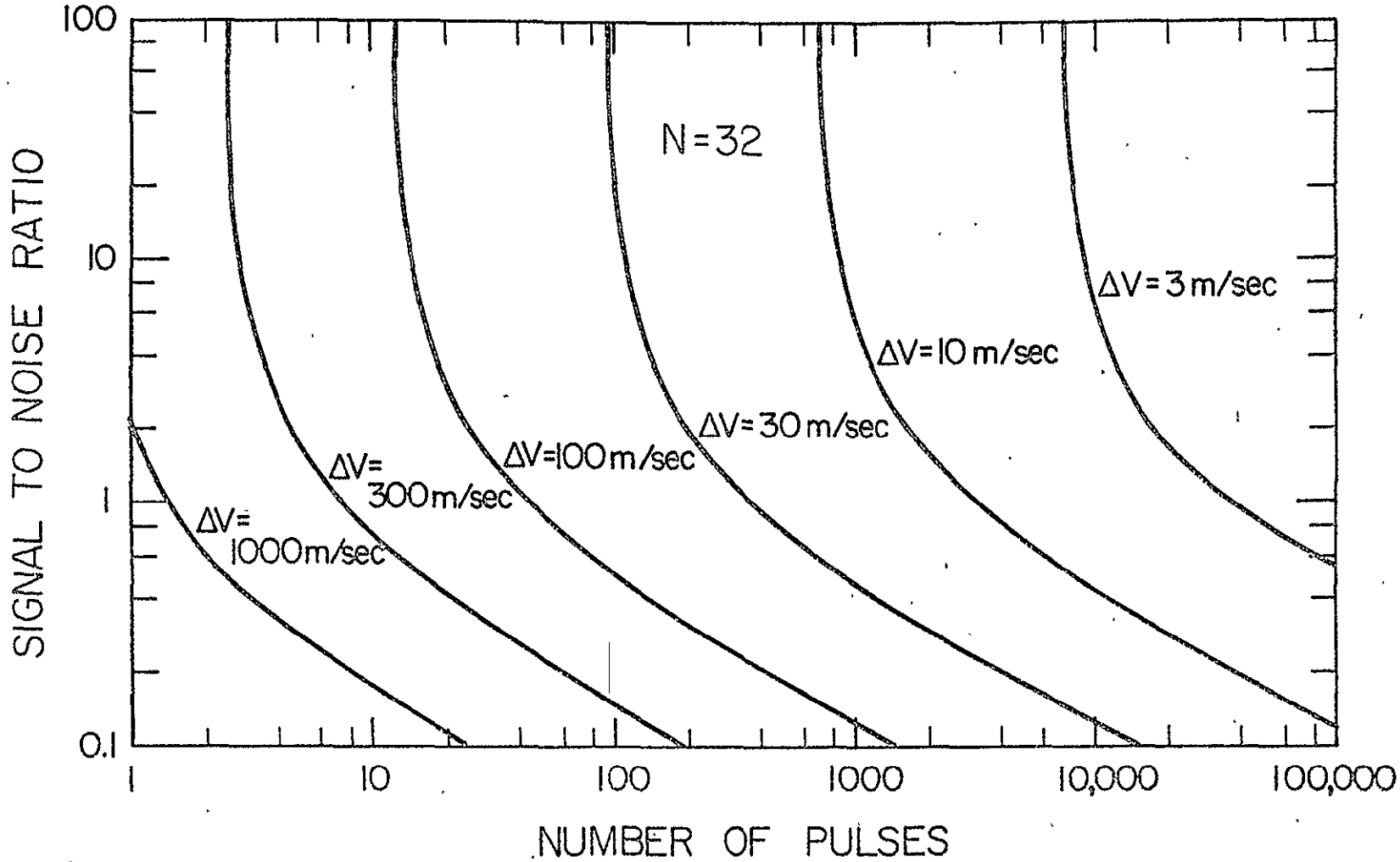
100
10
1
0.1
SIGNAL TO NOISE RATIO
N=32
ΔV=3 m/sec
ΔV=10 m/sec
ΔV=30 m/sec
ΔV=100 m/sec
ΔV= 300 m/sec
ΔV= 1000 m/sec
1
10
100
1000
10,000
100,000
NUMBER OF PULSES

Figure 8

DEPENDENCE OF ΔV (=UNCERTAINTY IN A SINGLE ESTIMATE OF THE DOPPLER VELOCITY)

ON THE SIGNAL TO NOISE RATIO

TABLE OF $\frac{\Delta V\,(SNR)}{\Delta V\,(SNR = 100)}$

SNR \ P	22500	22500	100	100	30	30	10	10	3	3	1	AVERAGE	EQUATION
T_e	1000	3500	1000	3500	1000	3500	1000	3500	1000	3500	1000		
T_i	1000	2500	1000	2500	1000	2500	1000	2500	1000	2500	1000		
100	1	1	1	1	1	1	1	1	1	1	1	1	1
10	1.07	1.07	1.04	1.13	1.13	1.16	1.13	1.15	0.97	1.10	1.04	1.09	1.09
1	1.85	2.43	1.95	2.94	2.08	2.92	2.05	2.60	xxx	xxx	xxx	2.35	2.21
0.1	9.59	16.3	12.6	21.0	xxx	xxx	xxx	xxx	xxx	xxx	xxx	24.9	24.8

$$\text{EQUATION} = \left[\left(1 + \frac{1}{SNR}\right)^2 + \left(\frac{1}{SNR}\right)^2\right]^{\frac{1}{2}}$$

NOTE - VALUES OF $\Delta V > 475$ METERS/SEC ARE DELETED FROM THE TABLE

Table 8

DEPENDENCE OF ΔV (= UNCERTAINTY IN A SINGLE ESTIMATE OF THE DOPPLER VELOCITY)

ON THE NUMBER OF PULSES

TABLE OF $\frac{\Delta V\ (P)}{\Delta V\ (P = 22500)}$

P \ SNR	100	100	10	10	1.0	1.0	0.1	0.1	AVERAGE	EQUATION
T_e	1000	3500	1000	3500	1000	3500	1000	3500		
T_i	1000	2500	1000	2500	1000	2500	1000	2500		
1	240	356	234	xxx	xxx	xxx	xxx	xxx	277	362
3	171	216	155	222	121	xxx	xxx	xxx	177	157
10	69.6	89.5	73.4	96.5	77.2	95.7	xxx	xxx	83.7	68.6
30	32.7	40.1	34.5	43.8	36.8	48.3	xxx	xxx	39.4	34.5
100	16.5	16.7	16.2	17.7	17.4	20.2	21.7	21.5	17.5	17.1
22500	1	1	1	1	1	1	1	1	1	1

$$\text{EQUATION} = \left(\frac{22,500}{P}\right)^{\frac{1}{2}} \left[1 + \left(\frac{2}{P}\right)^{\frac{1}{2}}\right]$$

NOTE - VALUES OF $\Delta V > 475$ METERS/SEC ARE DELETED FROM THE TABLE

Table 9